École Polytechnique Fédérale de Lausanne

Master's Thesis

ME-599

Feasibility analysis and preliminary design of a Lunar Reconnaissance Drone

Author:
Vincent Pozsgay

Project Supervisor:
Dr. David Rodriguez

Responsible Professors:
Prof. Colin Jones
Prof. Jean-Paul Kneib

June 23, 2022

Abstract

This thesis presents the feasibility analysis and preliminary design of a new Lunar Reconnaissance Drone. The system's objective, which is composed of the drone and a service station, is to assist a large-scale rover mission into low-light zones of the Moon such as the permanently shadowed regions (PSR). The drone uses a flash Lidar to obtain 3D high-resolution maps and transmits them to the rover, once docked on top of the service station. A risk analysis is performed, which concludes that the propulsion subsystem, the thermal control, and the mapping instrument are the most critical components of the mission. Nonetheless, throughout the project, no unfeasible aspects were encountered. All the subsystems are designed, with a focus on the propulsion system, followed by a first 3D model of the drone. A flight simulator is developed, and gives the optimal flight conditions, following the system's requirements. It leads to a flight time of 120.4 s, and fuel consumption of 1.86 kg for each flight. From this preliminary design, the estimated mass of the drone is 16.96 kg.

Acknowledgement

I would first like to thank and express my gratefulness to my thesis supervisor, Dr. David Rodriguez. He helped me a lot, by providing constructive and insightful advice and guidance throughout this project. He was always available whenever I was stuck or heading the wrong way, and helped me with sympathy and goodwill. It was a pleasure to work on this thesis under his supervision.

I would also want to thank Prof. Colin Jones who has accepted to be my academic supervisor, and Prof. Jean-Paul Kneib for hosting me within eSpace, without whom this Master's project would not have been possible.

I would like to thank Prof. Colin Jones and Prof. Hiroyuki Koizumi for attending my midterm presentation and giving me valuable feedback which I could include in the second part of my thesis.

Finally, I want to thank again David Rodriguez for reading and giving me feedback on my drafts, as well as Franzisca Haller von Hallerstein and Dr. András Pozsgay for proofreading my final report.

Contents

List of Figures

List of Tables

Glossary

- ADCS: Attitude Determination and Control System
- AGL: Above Ground Level
- CONOPS: Concept of Operations
- COTS: Component Off-The-Shelf
- DoD: Depth of Discharge
- EPS: Electrical Power System
- ESA: European Space Agency
- FMEA: Failure Mode and Effects Analysis
- FoV: Field of View
- HK: Housekeeping
- IMU: Inertial Measurement Unit
- LIDAR: Laser Imaging, Detection, and Ranging
- LV: Launch Vehicle
- NASA: National Aeronautics and Space Administration
- OBC: On Board Computer
- PSR: Permanently shadowed regions
- SE: Systems Engineering
- TRL: Technology Readiness Level
- UHF: Ultra High Frequency
- VHF: Very High Frequency
- VIPER: NASA's Volatiles Investigating Polar Exploration Rover
- WPD: Waypoint Driving

1 Introduction and context

Around 50 years after the first step was taken by Mankind on the Moon, going back is one of the current goals of space missions. The Artemis program was developed for this purpose, but this time, astronauts plan to return and stay to build Moon bases for further research. This requires extra exploration of the Moon, notably to obtain potential locations for the bases, for which the discovery of ice would enable the astronauts to stay for a long time autonomously. The exploration is currently planned to be conducted by wheeled rovers taking in situ measurements for ice search.

The upcoming exploration missions will be led by the VIPER rover, developed by NASA, which will start its operations in 2023, and is specially designed to try to find ice in specific regions of the surface of the Moon, the permanently shadowed regions (PSRs). These kinds of rovers, commanded by operators on Earth, move very slowly and proceed gradually along the surface of the Moon. VIPER's speed is around 10 to 20 centimeters per second when traveling to a pre-planned destination, and slows down to 5 to 10 centimeters per second in operations [1]. This means that the exploration takes a great amount of time, but the difficulty is that the rover cannot stay in challenging places such as permanently shadowed regions for long periods of time, especially due to the absence of sunlight, its source of energy.

Precise knowledge about the terrain is then crucial to plan and optimize the Rover's route. Acquiring this insight often relies on limited-resolution satellite data from lunar orbiters, data that is sufficient to be used by this type of rover in standard conditions, but is very limited in regions with little lighting such as PSRs. The need for a long-range, lightweight, simple, and efficient scouting method is then becoming more and more apparent.

Airborne robotic systems are currently being tested and deployed on Mars, with NASA's Ingenuity helicopter.

The goal of this project is to study the feasibility and to give a preliminary design of a compact and lightweight lunar reconnaissance drone. The latter's goal is to assist a large-scale lunar rover, such as VIPER, by providing high-precision mapping data of extreme shadowed terrains of the Moon. The rover could then use these maps to efficiently plan its trajectory in these challenging zones. The main design objectives for this drone are to provide high-resolution maps of the regions of interest, in a reliable, simple, and low-cost way.

Even if this analysis is centered on the drone's design, a service station, which is the interface between the drone and the rover, is also considered in this thesis. This base will be used as a shelter for the drone when it is not flying, and a refueling and power charging station, to prepare the drone for the next flight.

During the operating phase, the drone will take off the service station, which is attached to the top surface of a rover. The drone will then fly over a zone of the PSR, while mapping it with an onboard instrument, before coming back to land on the service station. The latter is used to transmit the mapping data to the rover, which can then plan a trajectory and move inside the PSR to take in-situ measurements.

This thesis follows the work started by Thomas Pfeiffer and Erik Uythoven [2].

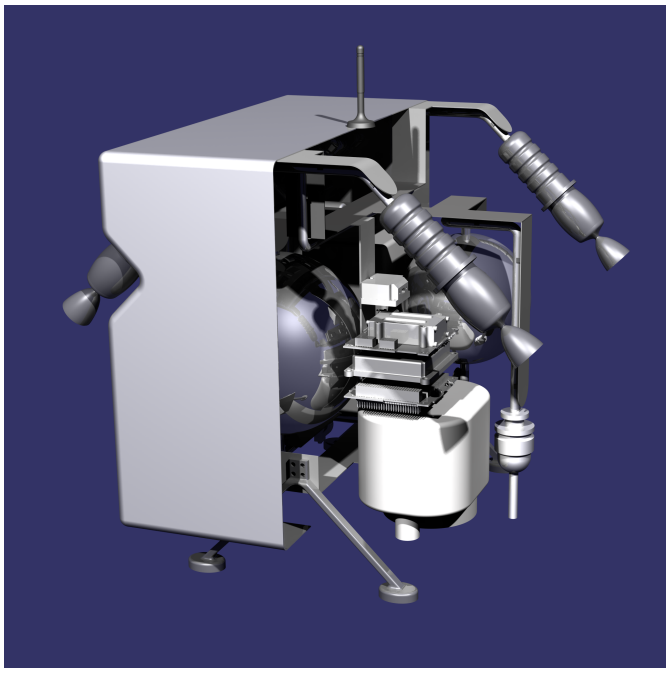

Figure 1: Inside view of the Lunar Reconnaissance Drone

2 Exploration of extreme locations on the Moon

This section gives an overview of the lunar environment and its challenges for exploration vehicles. It is mainly based on the article *The Moon in a nutshell* by David Rodriguez [3], and NASA's *Lunar engineering handbook* [4]. As the Lunar Drone's objectives are set to assist NASA's VIPER rover in permanently shadowed regions, this section focuses mainly on these zones, and potential other use cases for the drone, lunar lava tubes and their skylights.

Figure 2: Shackleton crater, taken by the advanced Moon Imaging Experiment (AMIE) on board of the SMART-1 spacecraft (ESA)

In the absence of a strong magnetic field, and with the Moon's gravity being small due to its low mass ($g = 1.62\,m.s^{-2}$), the Moon's atmosphere is extremely thin, even almost non-existent (its density is only $3 \cdot 10^{-15}\,bar$). Even though it can be useful for flying vehicles in certain aspects, as there is no friction, it also means that innovative solutions are needed to generate lift. This lack of a strong magnetic field also implies that a high dose of electromagnetic and particle radiation strikes the surface of

the Moon. These radiations, coming from the Sun for most of them, can damage the electronic components, especially the processor and the memory. Appropriate shielding and radiation hardened components are needed to mitigate these damages.

Due to a low albedo of 0.07 to 0.1 on average, most of the incoming solar energy is absorbed by the Moon's surface. This effect combined with the lack of atmosphere implies a huge temperature difference between day and night, with respective averages of $107°C$ and $-153°C$. This also plays a role at smaller scales, as the sun-exposed and the shadowed faces of the same object present a large temperature difference. This also means that the zones which receive no direct sun exposure, stay extremely cold.

This is the case for the Permanently Shadowed Regions (PSRs). These are areas located in the polar regions of the Moon. Due to the low inclination of the Moon's rotational axis, some craters never see the light rays coming from the sun. In these regions, the temperature can drop as low as 25 to 70 K [5][6]. The liquid water, that could have existed on the Moon, evaporated and escaped the lunar surface, however, frozen water could have stayed in these cold regions for a very long time. Even if NASA's Lunar Reconnaissance Orbiter suggested clues for the presence of ice, no in-situ measurement has been made to completely prove its existence.

If the presence of significant quantities of frozen water is proven, this could be highly beneficial for lunar exploration, as it could provide an ideal location for human settlements. Indeed, this water could be drunk by astronauts, used to grow plants and food, and the splitting into hydrogen and oxygen could provide breathable air or even rocket fuel. This would allow for autonomous lunar bases.

On top of that, other potential locations can be considered for Moon bases: the lunar lava tubes and their skylights, which are the remains of old volcanic activity. From JAXA's SELENE orbiter's images in 2009 [7], and NASA's Lunar Reconnaissance Orbiter in 2010 [8], pits were observed, which are believed to be skylights, lava tubes' openings. It is theorized that lava flowed beneath the surface and created hollow cavities that can extend for several kilometers. When the diameter of the cavities is too important, some zones collapse, and skylights appear, which are circular holes revealing the existence of these underground tunnels, as seen in figure 4.

Strong evidence of these skylights was obtained from orbiters images, but they have never been explored. These lava tubes could provide other potential locations for human-occupied bases. Indeed, the temperature in these tubes is much more homogeneous than on the surface, at around $-20°C$, removing one big challenge for these habitations [9]. Moreover, being underneath the surface of the Moon, lava tubes would provide natural protection from the high dose of radiation, but also the incessant meteoroid shower, caused by the lack of atmosphere to consume them.

Furthermore, the other big challenge for lunar vehicles is dust. The upper layer of the lunar surface is composed of regolith, which is dust and rock fragments, with a

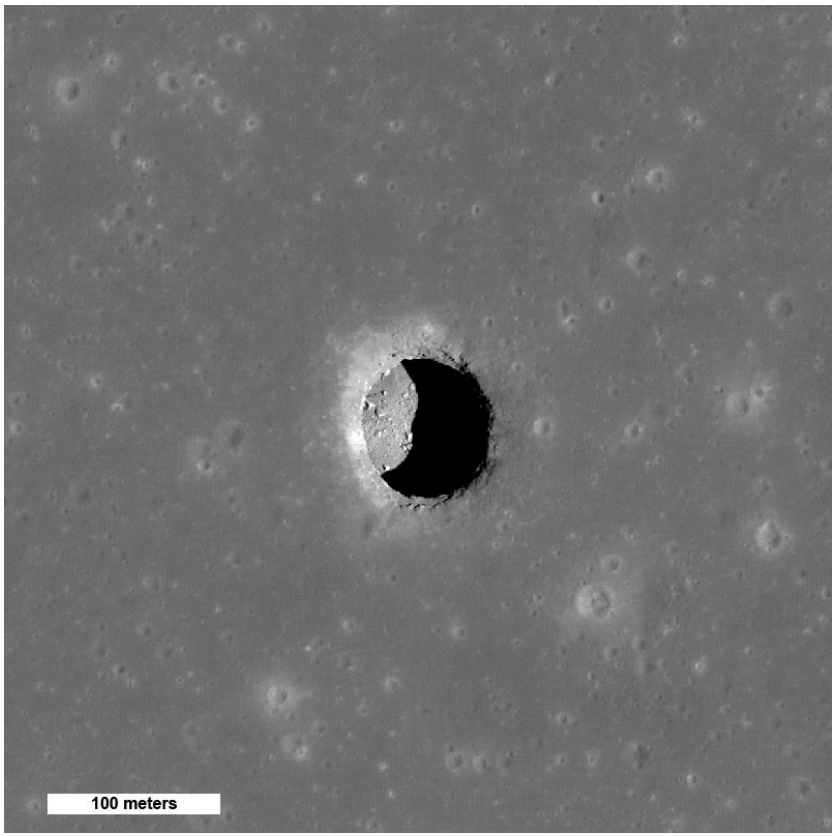

Figure 3: Mare Tranquillitatis pit crater taken from NASA's Lunar Reconnaissance Orbiter (NASA/GSFC/Arizona State University)

particle size of 20 μm and a density of around 1.5 $g.cm^{-3}$. Lunar dust is electrostatically charged due to the high dose of radiation and therefore adheres to the equipment used on the Moon. Dust dispersion is another issue when using moving parts, as it can go into the mechanisms and damage them. Being electrostatically charged, it can stick to optical parts reducing their accuracy, or cover solar panels reducing their power output.

3 State of the art

3.1 Lunar and PSRs maps

The main solution currently used to obtain mapping data of the Moon is the observation from in-orbit spacecrafts. Dozens of missions have been sent in this regard, to gain a better understanding of the lunar surface. The resolution of the maps obtained kept increasing, however, these definitions stay poor in low light zones, such as PSRs. The Lunar Reconnaissance Orbiter, launched in 2009, has the capability to obtain images of the Moon with a resolution up to $0.5m/px$ with its Narrow Angle Camera [10]. However, even with the recent help of deep learning to enhance the resolution, it stays very limited in PSRs with the smallest detection size of 7 to 10 meters [11]. ISRO's Chandrayaan-2 Orbiter High Resolution Camera (OHRC), which was launched in 2019 has a ground sampling size of $0.3m$ but needs a sun elevation angle of more than $5°$, and is therefore not suitable for PSRs [12]. JAXA's orbiter SELENE has among its objectives to observe the polar regions of the Moon, but its maximum resolution is $20m/px$ [13].

Therefore, even if new missions and cameras are built especially for PSR observation, such as NASA's ShadowCam on the Korean Pathfinder Lunar Orbiter, with a resolution of $1.7m/px$ [14], the lunar ground's images are getting better, but are still far from sufficient to plan trajectories accurately for rover missions' in-situ operations in low light regions of the Moon.

3.2 Exploration vehicles

The miniaturization of mechanical and electrical components has led to an increase in the development and the use of lightweight and compact aerial vehicles as means of exploration. On the surface of the Earth, these drones become very common and widely used for exploration, but also other purposes such as movie screening, or even delivery services.

The operation of lightweight aerial vehicles out of the Earth's atmosphere started only very recently, with the flight of JPL's Ingenuity helicopter, the first extraterrestrial vehicle of its kind. It has proven to work well on Mars, but its lift-off depends on a propeller system that demands the presence of an atmosphere, which is way too thin on the Moon. To this day, very few projects have examined such missions on the Moon and there are no existing vehicles adapted for it.

For the time being, the potential exploration of challenging zones of the Moon has been theorized and developed with another concept than fully aerial vehicles: lunar hoppers. These potential solutions solve the problem posed by the lack of atmosphere by using mechanical parts to take off, translate, and descend toward different landing zones. The most advanced lunar hopper project is Micro Nova, developed by Intuitive

Machines and recently funded by NASA [15]. This vehicle, some details of which are still undisclosed, aims to survey PSRs and measure their temperatures, by successive jumps inside the craters.

These kinds of lunar hoppers however encounter some limitations. As the payload mass is limited to less than $1kg$ for this hopper [16], three-dimensional precise imaging is not possible since this is insufficient to embark the necessary instruments, as seen in section 8.2.2. On top of that, the drone hops are close to the ground, which is not suitable to obtain images of large areas, hence not adapted for mapping and delivering the map to a rover to plan a route which will be used to perform in-situ measurements of the ground. As these hoppers need to land on the surface of the Moon, and especially inside PSRs which are extremely cold, additional thermal loads can also be added.

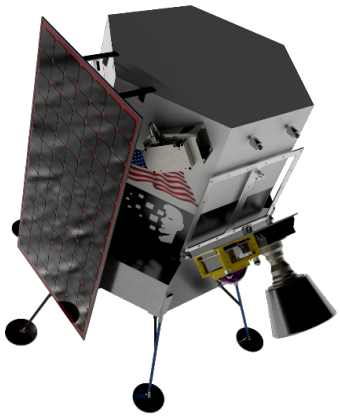

Figure 4: Intuitive Machines' Micro-Nova lunar hopper

The Lunar Reconnaissance Drone presented in this thesis is also inspired by reconnaissance drones and solutions used on Earth, namely regarding mapping techniques, which are usually equipped with optical or infrared cameras. Recently, laser imaging, detection, and ranging (Lidar) systems have often been added as mapping sensors for reconnaissance drones. For the propulsion and the other subsystems of the drone, the design is also inspired by CubeSats or microsatellites, which often have similar needs and requirements. For cost, reliability, and simplicity reasons, the majority of the components used in this preliminary design are off-the-shelf components designed for this type of satellites. No completely new components or technologies are required, which is favorable for feasibility.

4 Mission definition and objectives

This project is mainly linked to the needs and requirements of NASA's VIPER Rover, expected to be launched in 2023. The goal of this mission will be to explore a permanently shadowed crater, located near the South Pole of the Moon, with the main objective being to try to find ice in this region [17][1]. As mentioned in the previous sections, the two main challenges encountered are the extreme topography and the total absence of sunlight, which hinder the exploration capabilities of the rover. In this regard, a lunar reconnaissance drone, providing precise 3D maps to help plan the navigation in advance, could help tackle these limitations and increase the capabilities of the rover.

The main mission statement, which was defined at the beginning of the project [2], is therefore expressed as :

Assist a lunar rover mission in PSRs or extreme topography with a compact lunar reconnaissance drone module.

From the mission definition, the following objectives of this study are defined:

- Propose a conceptual design of a lightweight and compact lunar drone module for scouting and exploration (localized high resolution mapping) purposes, to assist a large-scale lunar rover mission in inaccessible or extreme environments.
- Lay a foundation for quick and simple means of exploration for future Moon missions.
- If possible, the drone should be reusable, modular and adaptable.

In this context, high resolution mapping is defined as a mapping of resolution smaller or equal to the characteristic length of a rover. This could for example be the radius of the rover wheel, a few tens of centimeters [2].

5 System architecture

This section presents an overview of the drone from the system's point of view. All the components that are described in this section and their functioning will be presented in more detail in the drone design section 8.2.

5.1 System decomposition and functional analysis

The drone and the service station are decomposed into different subsystems, with their main functions in table 1. The selected solutions are introduced in the last column, which are all justified in the following sections of this analysis.

5.2 High-level requirements

A set of high-level requirements are defined, based on the mission definition and main objectives. The requirements' definition started last semester during the preliminary analysis of the project [2] and was completed during this semester, mainly from the results of the risk analysis (section 6).

Figure 5 gives an overview of the most important requirements needed to satisfy the mission objectives. The full set of requirements, along with the verification method, is attached in the appendix A, which contains the requirements for the drone and the service station. These requirements are still preliminary with unknown values and are subject to change in the later phases of the project.

As for the solutions presented in the functional analysis, these requirements are justified in the following sections of this thesis.

Requirement type	Requirement description
Functional	The drone shall provide 3D mapping data to the service station
	The service station shall process the mapping data
	The drone shall be able to take-off, fly, and land autonomously
	The service station shall provide fuel and power to the drone
Performance	The payload's mapping resolution shall be better than 0.5 m/pixel
	The maximum horizontal flight velocity shall lie below 50 m/s
	The drone shall flight at 50 m (± 10 m) during the mapping
Constraints	The drone shall fit in the cover of the service station
	The service station's horizontal dimensions shall be less than (1.5x1.5)m²
	The drone's mass must be less than 20kg
Environmental	The drone shall resist the lunar environment during flight
	The service station shall protect the drone from radiation and low temperatures

Figure 5: High-level mission requirements

System	Subsystem	Functions	Solution
Drone	Propulsion	Provide lift to the drone	4 monopropellant thrusters
		Control the drone's attitude and trajectory	
	Payload	Generate 3D high resolution maps	Flash Lidar
	Power system	Energy source of the drone	No direct power generation, batteries charged before each flight
	Avionics	Store mapping data	OBC's internal memory
		Control all the electronic components	OBC
		Determine the drone's attitude	Use Flash Lidar's data combined with IMU
	Communication	Transmit mapping data to the service station	Wired communication
	Thermal control	Keep the components' temperature in their operating ranges	Thermal straps, patch heaters
	Structure	Keep all elements together	Carbon fiber structure
Service Station	Power system	Provide electrical energy to the drone	Generate electricity with solar panels and relay it to the drone
	Avionics	Process mapping data	Service station's OBC
	Communication	Collect mapping data from the drone	Wired communication
	Thermal control	Keep the drone's temperature in its operating range when not flying	Insulating cover
	Structure	Protect the drone from radiation and micrometeorites	

Table 1: Functional decomposition and selected solutions

5.3 System block diagram

This section presents a high-level schematic representation of all the components of the drone, with their data, power, and fluid interactions, as well as the external interfaces with the service station. All these elements are shown in figure 6

The system is mainly divided into two parts, the propulsion subsystem, and all the electronic components.

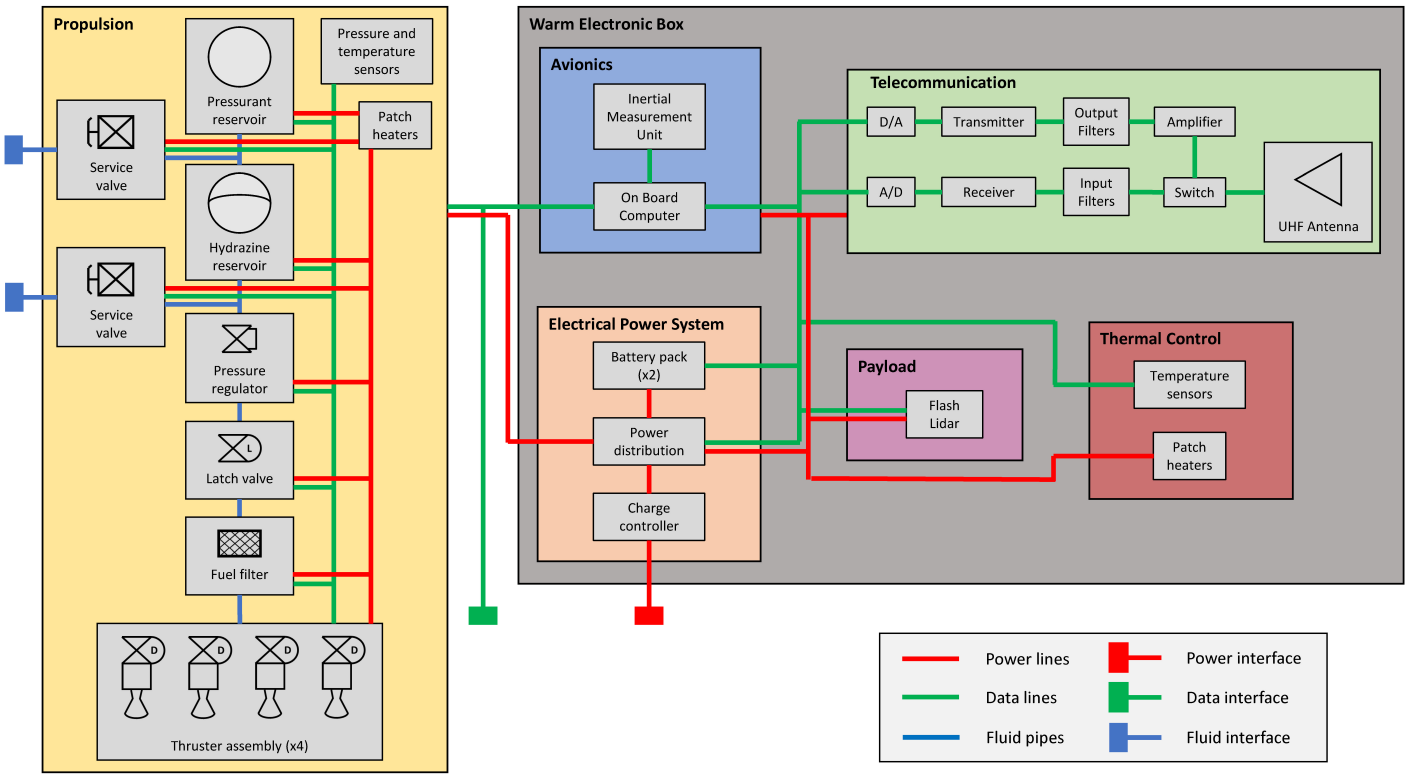

Figure 6: System block diagram of the drone

On the propulsion side, the main components are four thrusters assemblies, which contain one thruster, one catalyst with its heater, and a dual seat valve. The fuel storage and distribution include the reservoirs for the fuel and the pressurant, and all the hydraulic components required to control the flow from the tanks to the thrusters. The design of the propulsion system is presented in detail in section 7.1.

All the electronic components are placed together in a warm electronic box. These components having similar thermal range requirements (see section 8.2.5), they are all placed in a warm box that protects them from radiation and provides thermal control.

As the most critical components are in the same place, this minimizes the power consumption for the thermal control system. This will also help the integration, assembly and troubleshooting phase, as explained in section 7.3.

All the lines on the diagram represent interfaces between the different components. The electrical power system is connected to every active component, as it distributes the energy previously stored in the drone's batteries. In particular, it is connected to every electronic component, to every active component of the propulsion subsystem such as the valves or the thruster's heaters, and to the thermal control, which will generate heat in the desired locations with patch heaters. The drone has no internal power generation method, as it will be charged by the service station between each flight.

The onboard computer is the central part of the drone for the data aspect. As commonly used for spacecraft, mainly for reliability reasons [18][19], centralized data architecture is used, with all the components connected to the onboard computer. The OBC then sends all the commands to the components. It also receives housekeeping data such as the temperature or pressure from the different sensors, and stores the mapping data gathered by the flash Lidar on its internal memory during the flight. The possibility of having a separate control board for the propulsion subsystem is nevertheless evaluated in section 8.2.

Fluid interfaces are present only in the propulsion subsystem, where the pressurant applies a load on the fuel to control its flow with precision, from its tank to the thrusters, passing through all the needed fluid components.

The external interfaces are here to link the drone to the service station, once docked. As there is no way for the drone to generate power internally, a power interface is present to gather electricity that was previously generated by the rover and distribute it to the drone's batteries. The electrical power system will then distribute the power from the batteries to the other components during the flight.

The data interface between the drone's and the service station's onboard computers is mainly used to transmit the data collected during flight, especially by the flash Lidar, to the rover, which will process them to obtain the high-resolution maps. Commands or software updates can also be transmitted by this interface when the drone is docked.

Finally, two fluid interfaces connect the fuel storage system to the base. As the drone flies with only the amount of fuel necessary for one flight, it will need to be refueled before each operation. To do so, the fuel and the pressurant reservoirs are connected to larger tanks on the service station with two fill-and-drain valves.

5.4 Concept of operations and operating modes

The diagram in figure 7 presents the concept of operations (CONOPS) of the drone, which is a high-level sequence of operations that the drone will follow. It is split into two, with the docking mode on one side, and the flying mode on the other side. In

each of these modes, when a critical operation appears, a verification is made and in case of a problem, a safe mode is initiated. This diagram only presents the fundamental high-level operations, the full version of the concept of operations is attached in the appendix 45.

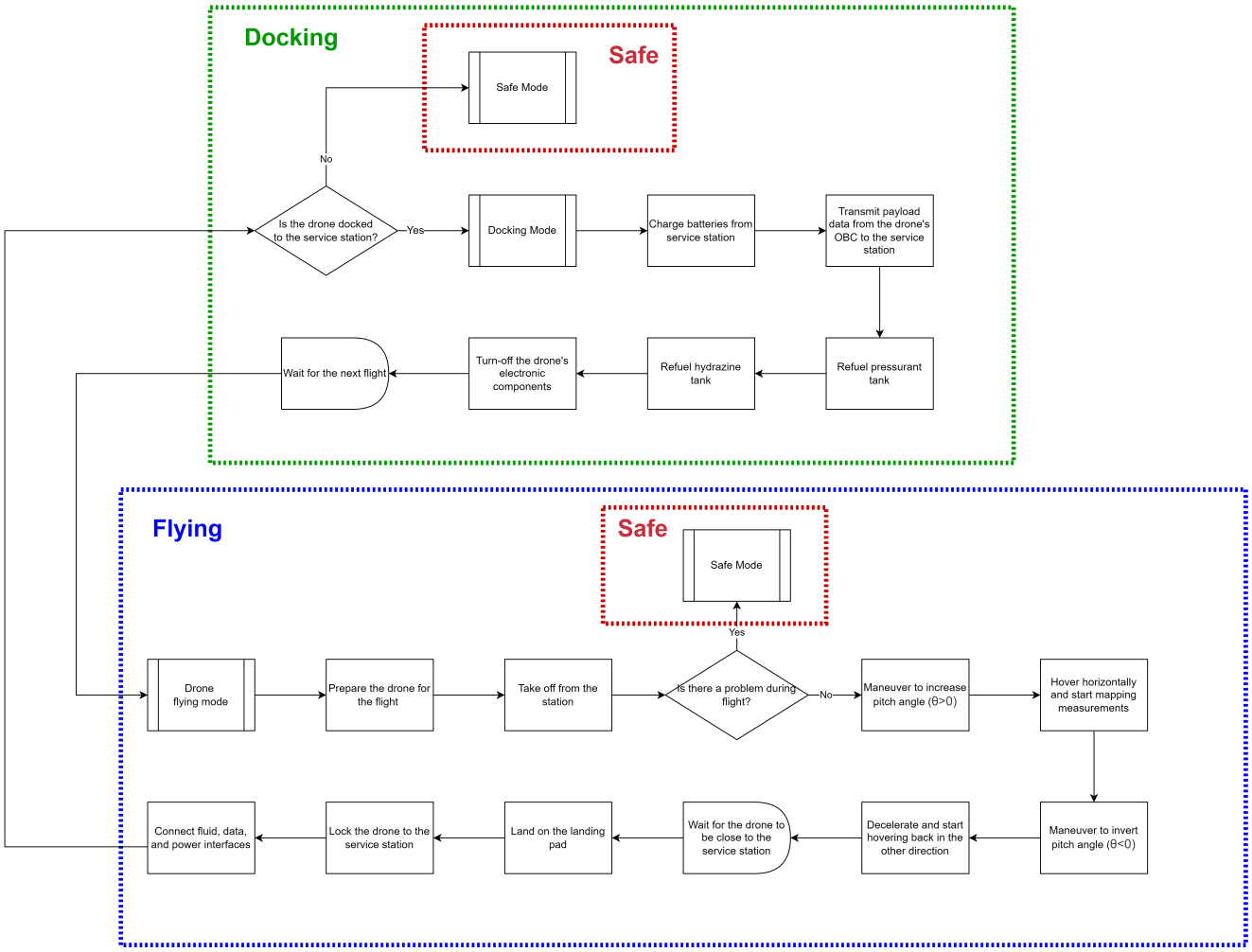

Figure 7: High-level Concept of Operations of the drone

Two safe modes exist, first the drone safe mode, which tries to solve the problem internally with the drone's OBC. If the drone is in flight, the goal of the drone safe mode is to abort the current flight and to go back to the base to land safely at the service station. If the drone is not flying, this drone safe mode is here to solve other potential problems, such as the impossibility to transmit the scientific data, to charge the batteries, to refuel the tanks, etc. If the problem cannot be solved internally, once docked, the system safe mode is initiated, which is commanded by the service station,

taking control of all operations.

In the flying mode, the thrusters are heated to be within their operating temperature range, then verifications are made to ensure that the drone can take off safely, and the flight can start. Note that more information on the flight strategy and trajectory is described in section 9. The flight trajectory is shown in figure 8, where only the takeoff and the hovering in one direction are represented, as the trajectory is symmetric. The four thrusters provide a predefined level of thrust to take off vertically above the service station. During the take-off thrust, when the drone is several meters above the base, a maneuver is made to increase the pitch angle, so that the drone starts to accelerate in the horizontal direction. The altitude is then stabilized vertically at $50m$ above ground level, with still a constant acceleration in the horizontal direction. The drone hovers with a constant thrust for the predefined time/distance. A maneuver is then made to reverse the pitch angle. The drone decelerates, stops, and starts the acceleration in the rover's direction. When close to the landing pad, a maneuver is made to decelerate. The thrust is then decreased to initiate the landing phase, a final maneuver is made to stabilize the drone at a zero pitch angle above the station, and the altitude decreases. In the final moments of the flight, the thrusters are reignited to ensure that the impact of the landing is minimal. The thrust stops, and the drone is locked to the service station, whose cover closes to protect the drone. Verifications are made to ensure that the drone is correctly docked to the station, the propulsion system can be turned off and the drone exits the flying mode.

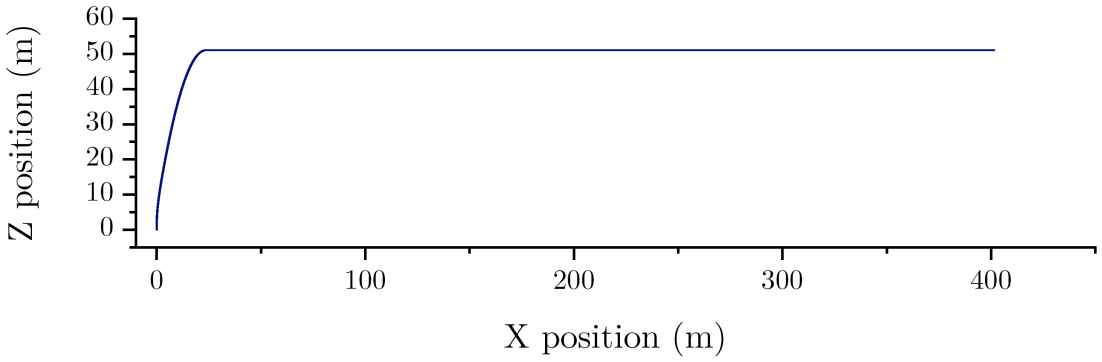

Figure 8: Drone trajectory

The docking mode's purpose is to protect the drone from radiation and provide thermal regulation when not flying. It is also here to collect the scientific data and to prepare the drone for its next flight. In the sequence of operations, after the landing, the batteries of the drone are charged, and then all the data collected by the drone during its previous flight is transmitted by cable to the service station. All the subsystems

of the drone can then be turned off or put in standby mode. The drone waits in this state for a command coming from the station to prepare for the next flight. When it arrives, the battery level is checked, and completed if too low. The fuel and pressurant tanks are refueled, all the subsystems are turned on, the cover of the service station is removed, and the drone is ready to fly. Note that the electrical interface between the drone and the service station is disconnected during the refueling, to avoid any fire in case of leakage during this critical phase.

This concept of operations allows determining when, and on which operations, failures can happen in the system. This CONOPS then allowed completing the risk analysis, which is presented in section 6.

5.5 System sizing

This section, which mainly results from the drone design (8.2), introduces the different system budgets. Each of the components is listed, with its mass, and power. Note that an attempt to define a preliminary cost budget was made, however, as the project is still in its very preliminary phase, a lot of uncertainty appears in the cost of the different components. Only the cost of off-the-shelf electronic components could be obtained, which represents a very small part of the overall cost, compared for example to the measurement instrument, a flash Lidar which is still in development.

The selection of all the components introduced in these budgets is justified in the later sections.

5.5.1 Mass budget

The mass of every component of the drone is presented in figure 9, with the mass budget of the propulsion subsystem only in figure 10. The majority of the components are commercially available ones, usually designed for small satellites. For all the components with uncertainty or which were designed during this semester, a component level margin of 20% is added. A global system margin of 20% is also added, as we are in the very early phases of the project [20][21][22].

The total estimated mass for the drone is then $16.96kg$ with $8.15kg$ for the propulsion system only, including $2.42kg$ of fuel and pressurant, at the beginning of each flight.

5.5.2 Power budget

The power budget of the drone during operation is presented in figure 11. The same margin method as for the mass budget is applied here for the in-house or uncertain components, as the system margin for the power budget is 10% [20][21]. During the flight, the estimated power consumption is then $324W$. Note that only one operating mode is considered in this analysis. It is the case because, during operations, all the components will be turned on together, thus consuming their design power together.

Subsystem	Mass (kg)	Subsystem margin (%)	Total Mass (kg)
Propulsion	8,1214		8,1214
Structure	1,5	20	1,8
Wiring	0,6	20	0,72
Payload	2	20	2,4
Telecommunication	0,0405		0,0405
Antenna	0,033		
Transciever	0,0075		
Avionics	0,149		0,149
On Board Computer	0,094		
Inertial Measurement Unit	0,055		
Thermal control	0,72		0,72
Patch heaters	0,1	20	
Thermal straps	0,5	20	
Electrical power system	0,184		0,184
EPS + battery pack	0,184		
Total without margin			14,1349
System level margin (20%)			2,82698
Total mass			**16,96188**

Figure 9: Mass budget of the drone

Component	Unit Mass (kg)	Number of units	Component level margin (%)	Total Mass (kg)
Fuel tank	0,91	1		0,91
Pressurant tank	0,4	1		0,4
Pressure regulator	0,34	1		0,34
Latch valve	0,1	1		0,1
Fill and drain valves	0,209	2		0,418
Valve heaters	0,01	4	20	0,048
Tank heaters	0,05	2	20	0,12
Propellant filter	0,056	1		0,056
Pressure transducer	0,075	2		0,15
Temperature transducers	0,01	2		0,02
Thruster assembly	0,59	4		2,36
Fuel lines	0,24	1	20	0,288
Dry mass without margin				5,21
Subsystem level margin (10%)				0,521
Dry mass				5,731
Propellant	1,86	1	20	2,232
Pressurant	0,154	1	20	0,1848
Wet mass				**2,4168**
Total mass without margin				7,6268
Total mass				**8,1478**

Figure 10: Mass budget of the propulsion system of the drone

When the drone is docked and protected by the service station, all the components are turned off or in standby mode and the power consumption is then negligible.

Component	Unit power consumtion (W)	Number of units	Component level margin (%)	Total power consumption (W)
Propulsion	206,768			206,768
Latch valve	8	1		
Valve heaters	5	2	20	
Tank heaters	5	2	20	
Pressure transducer	0,6	2		
Thruster assembly	36,16	4		
Valve	25,1			
Valve heater	4			
Catalyst bed heater	7,06			
Payload	42			42
Flash Lidar	35	1	20	
Telecommunication	6			6
Transciever	6	1		
Avionics	2,4			2,4
OBC	0,4	1		
IMU	2	1		
Thermal control	12			12
Patch heaters	5	2	20	
EPS	1,2			1,2
Batteries heaters	1,2	1		
Total without margin				270,368
System level margin (20%)				54,0736
Total power consumption				**324,4416**

Figure 11: Power budget of the drone in flight

6 Risk Analysis

6.1 Methodology

As part of the feasibility analysis, the risk analysis is fundamental in order to gain a better understanding of the challenges of the project and to highlight the aspects that need the most care during the design. The risk analysis is made on the whole system (drone and service station), but a deep focus is given to the risks associated with the drone, as it is the central topic of this thesis. The risk analysis' formulation was an iterative process, which started at the beginning of the semester and was completed after each phase of the work. For example, the definition of the CONOPS (5.4), helped to bring out the critical operations, which were linked to the risk analysis. The approach used during this work was the Failure Mode and Effects Analysis (FMEA) [20][23].

The full diagram containing the failure mode and effect analysis is presented in the appendix D, and is explained in this section. This FMEA classifies the failure modes by subsystems, but different subsystems can be interconnected, as explained later in this section. For each subsystem, the main potential failure modes are listed and associated with potential causes which can lead to them. To know what risk is more important and needs particular care in the design, a ranking has to be made. To do so, every failure mode is associated with a severity, and every potential cause is associated with a probability with the following grades [24]:

Severity rating:

- 1: Negligible: Operating conditions are such that personnel error, environment, design deficiencies, subsystem or component failure or procedural deficiencies will result in no effect on the systems function
- 2: Marginal: Failure may commonly cause minor effect on the systems function
- 3: Considerable: Failure may in some cases cause functions to stop system from fulfilling mission success requirements
- 4: Critical: Failure causes serious absence of required functions. Most mission success requirements will not be met
- 5: Catastrophic: System ceases to function, no mission success requirements can be met

Probability rating:

- 1: Extremely Unlikely: So unlikely that occurrence is negligible
- 2: Remote: Occurrence possible but unlikely
- 3: Occasional: Likely to occur at some point in lifetime
- 4: Reasonably Possible: Will occur several times in lifetime
- 5: Frequent: Likely to occur often

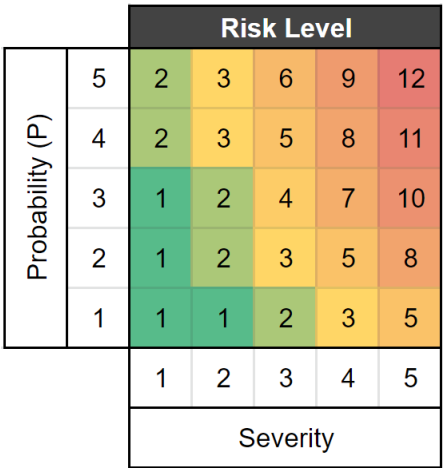

Figure 12: Risk matrix

These two ratings are then processed together in the risk matrix of figure 12 to define the overall risk level on a scale from 1 to 12. Each failure mode is attributed to

a reference number so that links can be made between the different subsystems if one potential cause has implications on multiple parts of the satellite.

If the risk level of a couple potential cause / failure mode is higher than 5, a mitigation strategy is defined. The risk analysis and the requirements are also interconnected, one can have an influence on the other, and this link is shown in the risk analysis diagram (Appendix D).

6.2 Lessons learned from the risk analysis and impact on the system

The most important part of the FMEA for this preliminary design and feasibility analysis is to understand what is its output, what implications it has on the design, and how to tackle the different challenges.

First, a look at other space missions, and particularly the reason why some of them failed, is taken. Studies have been made for satellites [25], collecting the statistics of mission failures. They concluded that for the spacecrafts with a propulsion system, the attitude determination and control subsystem using this propulsion is the most critical, with a rate of failure of 32%. This has to be kept in mind for this project, where the propulsion system plays a very important role. Special attention to the propulsion, controlling the trajectory and attitude of the drone, and the fuel storage system must therefore be taken.

From the risk analysis of this specific mission, three critical subsystems emerged and need particular care in the design and testing phase.

Propulsion and flight control: As previously stated, the main failure risk comes from the propulsion system and the flight control. To mitigate these risks, a flight simulator must be developed to fully understand how the drone will behave, and to optimize the flight trajectory. This simulator will also help develop strategies in case of off nominal situations, for example how to come back and land on the base in case of a thruster failure. External perturbations will also have to be modeled and applied to the simulation to understand how to control the drone in these situations. Fluid simulations are required to visualize the gases coming out of the thrusters, in order to avoid damaging the other components and mitigate the dust dispersion. Finally, intensive testing of the control algorithm and the components, especially the thrusters will be needed, to predict exactly what will be the behavior of the drone and prevent failures.

Thermal control: There is a major risk of underheating or overheating of some parts of the drone. Early thermal simulations were made [2], but in-depth thermal simulations will be needed, with the 3D design of the drone, to locate hot spots. The optimization of the heat flux inside the drone, and clever thermal design to distribute this heat, will be needed. Flight simulations coupled with thermal simulations will be done to meet the mission requirements in the shortest amount of time to stay in the

temperature's operating range of the components. Testing of all the components is required, especially the thrusters, to see how much heat is conducted to the interior of the drone.

Flash Lidar: The Flash Lidar is a key component because it is needed both for the measurements, and the take-off and landing, with the landing on the base being the most challenging aspect of the flight. Dust is the major potential risk for the optics, therefore fluid simulations are required to optimize the thrusters' placement on the drone, to mitigate this dust dispersion. On the service station's side, the development of a flame diverter is needed, with the association of fluid simulations and testing to predict how much, and where, the dust is dispersed.

7 Configuration and 3D design

This section introduces the configuration and the 3D design of the drone, based on the design of all components and subsystems, which will be justified in section 8.2. The requirements for the configuration mainly concern the maximum allowable volume of the exterior of the drone. The drone needs to be as compact as possible to be able to fit in the service station. For the moment the design of the service station is not defined, so the dimensions of the base are unknown, but an approximation can be derived from the VIPER rover, which is the reference rover used through this analysis. Its top surface is approx $1.5m$ x $1.5m$ [26], then if the service station is added on top of the rover, it will crop some of this available area. A requirement for the inside of the service station can then be stated as: "The drone's exterior dimensions in the horizontal plane shall be less than $0.5m$ x $0.5m$". There is more flexibility on the vertical dimension, so no hard requirement is formulated.

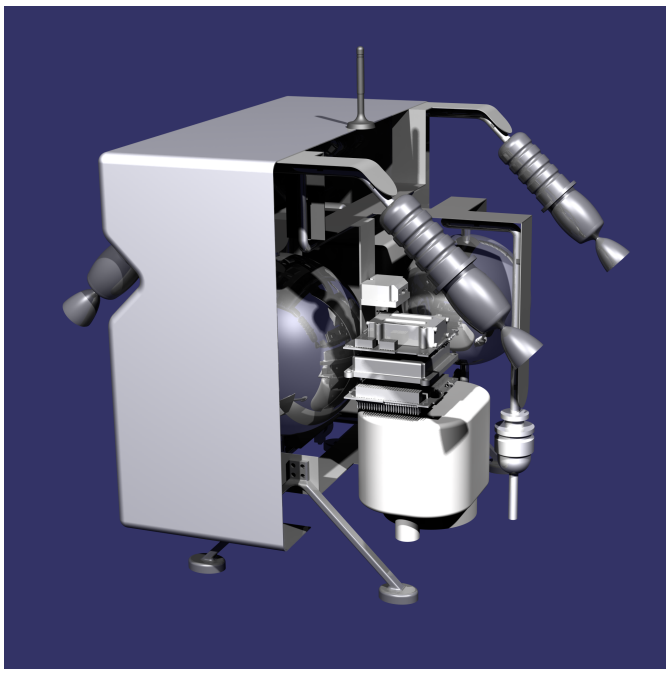

Figure 13: 3D configuration of the drone

The goals for the design are the following, in this order of importance. The drone shall be as compact as possible. It shall be easy to assemble and disassemble for the testing phase. Its center of gravity must be low, to be more controllable. The thermal distribution and the potential heat loads must be kept in mind, as well as the simplicity and reliability of landing and connection to the service station.

The configuration of the drone is inspired by MicroSat projects, as well as the con-

figuration of NASA's Ingenuity [27] and ESA's Sentinel 2 series [28].

An iterative method was adopted for the drone configuration. It started with the propulsion system, then the structure was added, and finally all electronics elements. Then the design goals were considered again to see if they were respected and what could be improved. Another iteration started again with the lessons learned from the last design. The final version of the configuration is presented in the next subsections.

All the elements used in this section are the ones introduced in the system sizing section (5.5) and justified in the drone design one (8.2). The 3D design of the components is taken from the constructors if available (for the EPS, IMU, and transceiver), other parts are drawn based on the constructors' specifications (for the OBC, Flash Lidar, thruster assembly, valves, pressure regulator, fuel filter), while the fuel lines, the structure, and the exterior panels are designed especially for our needs.

7.1 Propulsion system

The propulsion system is the central one in the configuration, as it is the subsystem with the most element, the bulkiest, and components from this subsystem are distributed in multiple places in the drone. Start the overall configuration with this subsystem.

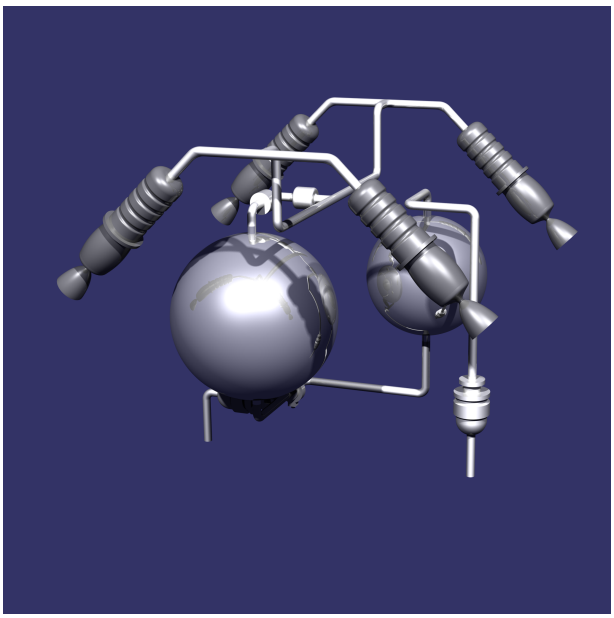

Figure 14: Configuration of the propulsion subsystem

The two tanks, for the fuel and the propellant, which are very bulky and heavy, are placed as low as possible in the drone to lower the center of gravity. Both tanks are

connected to the lower part of the drone, with fuel and drain valves. These connections protrude from the exterior surface of the drone and will have to be linked to the service station for refueling once docked.

The pressurant tank is linked to the fuel tank, through the pressure regulator, below the tanks, while the fuel tank is connected to the thrusters through the latch valve and the fuel filter, above the tanks. As justified in section 9, the thrusters are located on the top corners of the drone, with an angle of 45° from the y-z plane.

With this configuration, most of the fuel lines lie in two different planes, and the tanks are close to the lower surface of the drone. These tanks are arranged diagonally so that there is room for the electronic components on the other diagonal.

Note that in this preliminary configuration, the thrusters are placed with an angle of 45° from the y-z plane but aligned with the x-z plane. This configuration is adopted as adding another angle for the thruster will lead to an increase in the fuel consumption, as explained in section 9. The current requirements for the flight trajectory state that the drone shall be able to move in straight lines, and the actual design is adapted to this case. However, if in the future phases of the project some other trajectories are studied, this configuration will have to be reevaluated and the angle from the x-z plane could be modified.

7.2 Structure

The structure is mainly inspired by the design of ESA's Copernicus Sentinel 2a [29]. This satellite's structure is designed with a main composite plate on which all elements are attached, and the same approach is used here. As most of the fuel elements are positioned on two different planes, then two horizontal structure plates to hold them are present, with a vertical plate linking them. These are the principal elements of the structure, on which most of the forces will be applied during the landing (see section 8.2.7 and appendix F).

From the three main structural elements, small plates are attached, which are used to fix all the other elements, such as the thrusters, the fill and drain tubes, or the flash Lidar.

All the fluid lines are fixed to the structure plates using collars. With this solution, all the elements are firmly linked together, but some parts of the propulsion system can be easily disassembled for the testing phase.

Finally, carbon fiber legs are fixed to the bottom plate, which are inspired by ingenuity's legs [27]. After the landing, the position of the drone inside the service station must be extremely accurate to allow refueling, data, and power connection, therefore a guiding mechanism will have to be designed for the service station. The design of the legs is now imagined to fit in these guiding mechanisms, allowing the drone to be in a precise, fixed position, but will have to be updated when the exact specification of these

guiding mechanisms will be known.

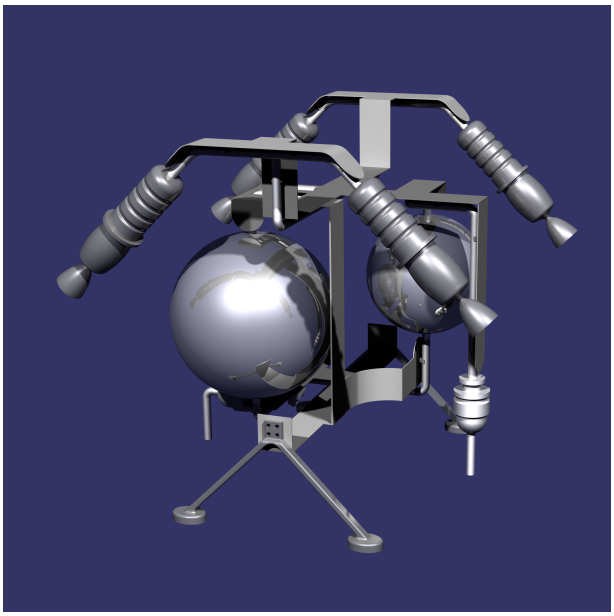

Figure 15: Configuration of the structure and the propulsion subsystem

7.3 Electronics

As all the electronic components have similar thermal components, the idea is to place them all together inside a warm electronic box. This box is placed at the lower position possible to have a low center of gravity, and also to be far from the thrusters, which are the hottest components of the drone. The Flash Lidar shall be placed on the bottom side of the drone with nothing obstructing its field of view.

In the design of the propulsion system, some room is left free, between the tanks, to fit the electronic box. It contains the optics of the flash Lidar, the OBC, the EPS, the transceiver, and the IMU. The box is screwed to the vertical plate of the structure so that it can be opened and disassembled very easily without complex operations. As mentioned in section 8.2, it is assumed that the optics and electronics of the flash Lidar can be separated. The optical part is placed in the main electronic box, while the other part of the Lidar is in a secondary electronic box, on the other side of the drone. This allows for a much more compact design, and a better mass distribution, which will facilitate the control.

Note that the possibility of having a separate board for the propulsion subsystem is evaluated in section 8.2. However, this board could be used only for testing and troubleshooting, and the propulsion system's operations could go back to the OBC, with a fully centralized architecture, during operations.

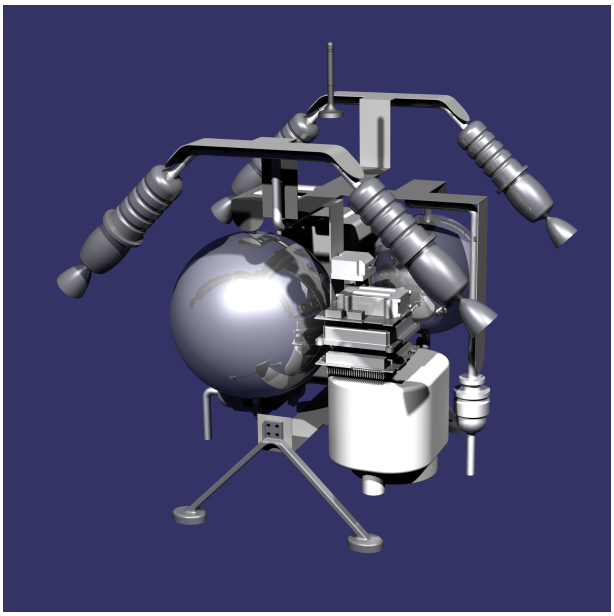

Figure 16: Configuration of the structure, the propulsion subsystem, and the electronic components

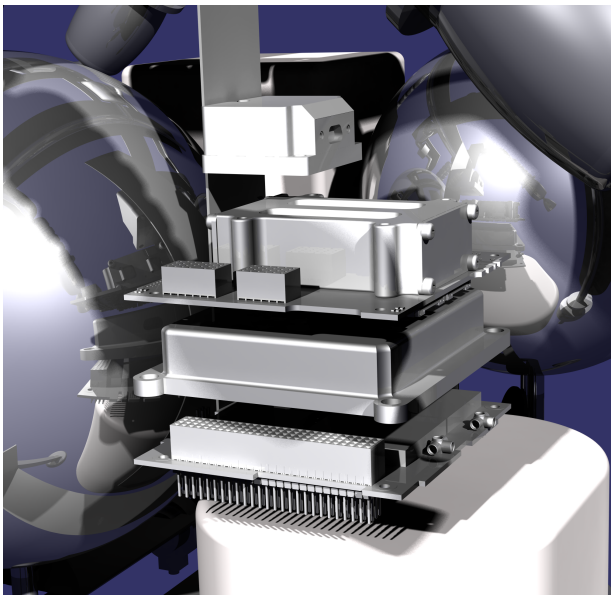

Figure 17: Configuration of the inside of the electronic box, including from top to bottom, the IMU, the EPS, the OBC, and the transceiver

7.4 Exterior design

The final configuration of the external design of the drone is shown in figure 18. Side panels are added to cover all the components, with only the thrusters, the antenna, and the interfaces coming out of these panels. The goal of this external layer is to protect the components from radiation and micrometeorites during flight, but is also crucial for thermal control, as seen in section 8.2.5. The exterior panels' material parameters (emissivity, absorptivity) are not defined yet, as they will have to be tuned from the results of the complete thermal simulations. However, it can be inspired by most satellite designs, which have similar thermal environments, and use multilayer insulation for most of them [30].

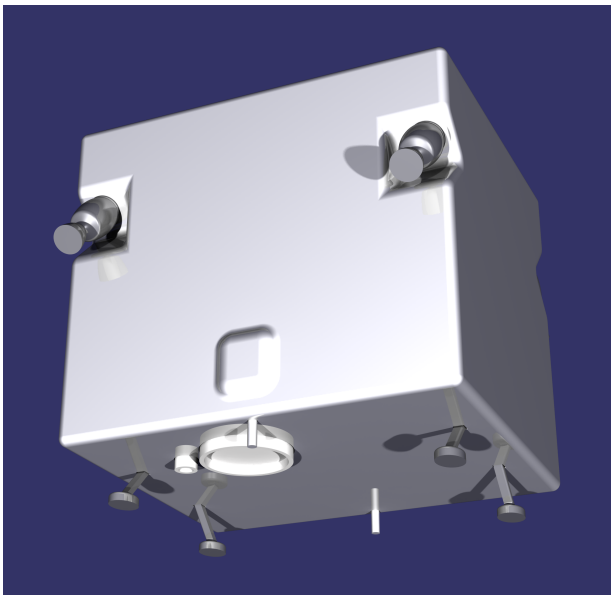

Figure 18: Exterior configuration of the drone

In the configuration obtained from the final iteration, the external dimensions of the drone are $450mm$ x $480mm$ x $378mm$, which fulfills the volume requirement.

8 System design and trade-offs

This section goes through the design of every subsystem, with the selection of all the components necessary for the system's operations. Different trade-offs are made to determine the best option in different conditions. The method used for these trade-offs is explained in appendix C, with the example of the thrusters' configuration.

8.1 Service station

This thesis was focused on the design of the drone, nevertheless, an overview of the subsystems and the function of the service station, mainly based on the work done last semester [2], is given in this section.

As introduced in the functional decomposition (section 5.1), the drone's service station has four main functions:

- Provide a shelter for the drone when not in use, i.e.:
  - Attach and secure the drone during the flight to the Moon and the rest of the rover mission with a reversible hold down and release system
  - Insulate the drone to prevent large temperature losses with a radiation cover
  - Connect the drone to the thermal system of the rover
  - Provide a shelter from the intense radiation dose and micrometeorites impacts
- Provide a take-off and landing base, including:
  - A flame diverter to direct the thrusters exhaust gas away from the rover
  - Features to ease the landing of the drone (for example optical markers or lights)
- Provide data connection to transfer the mapping data from the drone to the rover
- Allow for the refueling and recharging of the drone to make multiple flight possible and therefore have:
  - Propellant and pressurant tanks
  - Fuel line connection and disconnection systems
  - Power distribution system

The drone base shall be as compact and independent as possible so that it can be adapted to multiple mission scenarios, and fitted into a wide variety of rovers. The rover's requirements state that it shall be able to perform at least 10 flights. The service station shall then initially embark fuel and pressurant for at least 10 flights in its tanks. Based on the estimations from sections 9, 8.2.1, and appendix E, this corresponds, with a margin of 20%, to $26.68kg$ of fuel and $2.22kg$ of pressurant. From appendix E, the fuel and pressurant tanks must respectively have radii of at least $18.7cm$ and $13.1cm$ to

respect the drone's requirements.

The risk analysis introduced in section 6 also has implications on the service station design, as it showed the aspects that require the most attention. The main risk is that the drone cannot land and be docked properly to the station. The landing pad shall be designed with guiding mechanisms that allow for the maximum margin possible during the drone's landing.

A deep focus on the mechanisms is also needed, such as the drone's locking mechanisms or the cover's opening and closing mechanism. These moving parts are especially critical as dust could penetrate and damage them. Dust is also dangerous for all the connectors, a clever design will have to be made so that the power, data, and fluids can be transported between the station and the drone without losses, and without dust intrusion.

Thermal simulations and thermal design shall be investigated under the base's cover. It needs to maintain the temperature in the drone's operating range ($+10°C$ to $+50°C$, see subsection 8.2.5), for very long times, both in the shadow and in the sunlight. An efficient way to dissipate heat shall be designed, with direct sunlight on one side, and contact between the rover and the ground, which are different thermal conditions than the drone's ones, where the external heat is only provided and dissipated by radiation.

8.2 Drone

This section goes through every subsystem that is needed in the drone. For reliability, cost and simplicity reasons, each time it is possible, the components used are space proven and commercially available, with the original purpose of operating in CubeSats or microsatellites. As the environmental conditions and the requirements are similar for CubeSat and this lunar drone, these components were favored.

The design of the drone was also inspired by ingenuity [27] [31] [32], as even though the operating conditions are different, the mission objectives are similar.

8.2.1 Propulsion system

First, different strategies and technologies were evaluated to select the best one for trajectory and attitude control. Several trade-offs were realized, both from the analysis made last semester [2], summarized in figure 19, and in the flight strategy section (9), to find the best solution. The result of these analyses is that the best option, following the mission objectives and requirements, is to use four thrusters, located in the top corners of the drone, to control the take-off and landing, but also the trajectory and attitude. With this solution, only these four thrusters assemblies are used, without the need for additional attitude control thrusters, reaction wheels, or gyroscopes. The

trade-off method used for the choice between four thrusters and one main thruster with the addition of small secondary thrusters is discussed in detail in appendix C.

The trade-off between different propellants can be found for this mission [2], and concluded that monopropellant is the more suitable, mainly because of its simplicity and efficiency.

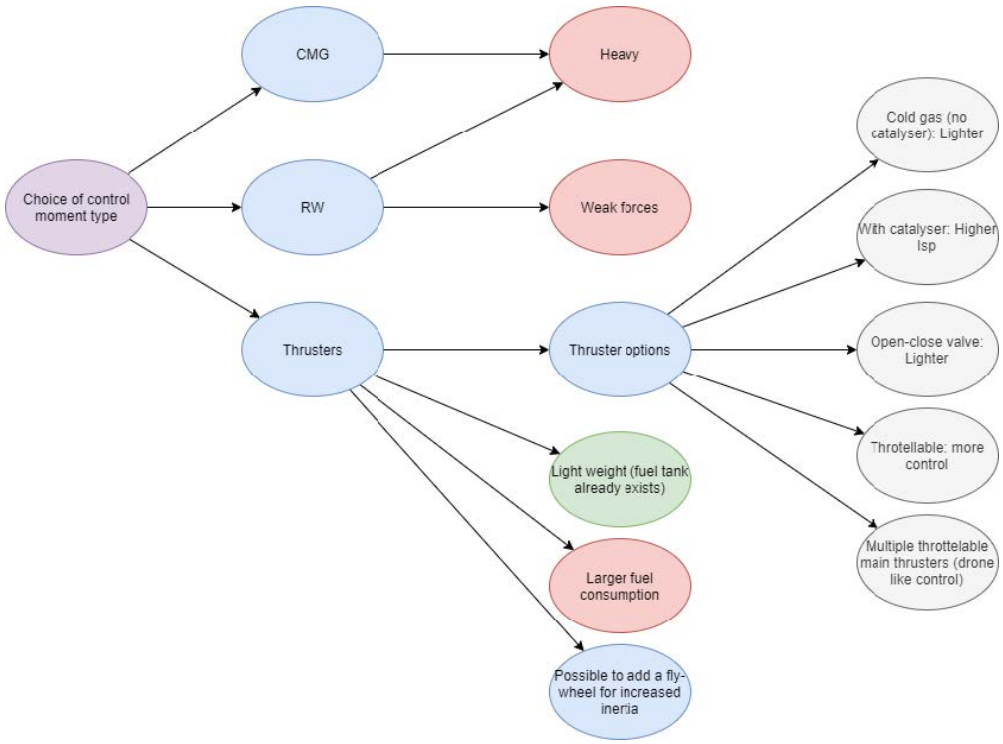

Figure 19: Choices and effects of spacecraft attitude control technologies [2]

Thrusters' placement has also been investigated in the early analysis [2]. It concluded that the best option was to place the thrusters on the top corners of the drone. Indeed, it mitigates well the dust generation and allows for simple and efficient placement of the Lidar's optical instrument. The thrusters are located way above the center of gravity of the drone, which simplifies the controllability, and quadcopter control algorithms can be used as references for the lunar drone's flight algorithm.

To mitigate the dust dispersion and the heat transmission from the thruster's exhaust gas, as explained in detail in section 9.6, the thrusters shall be angled from the y-z plane, as shown in figure 20. The angle β from this figure is referred to as the thruster's angle in this report. The angles α and β are further investigated in section 9.6, where optimization is made between the fuel consumption and the mitigation of

dust dispersion and optical measurements' perturbation.

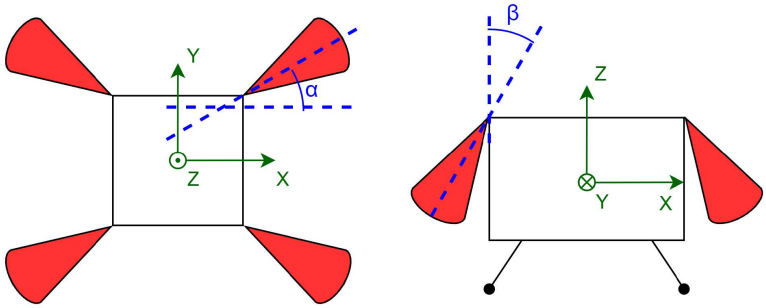

Figure 20: Top view (left) and side view (right) of the drone with its four thrusters (red). The x-axis is in the main direction of flight [2]

From section 9, requirements for the thrusters can be formulated as

- The thrusters shall be able to provide at least $35N$ of thrust during at least 5 seconds
- The thrusters shall be able to maintain a constant thrust of at least $20N$ during at least 2.5 minutes
- The thrusters shall be able to provide small thrust variations as low as impulses of $0.08N \cdot s$

The criteria that were taken into account for the selection of the thruster are, in order of importance: low mass, high specific impulse, flight proven if possible, low power consumption, low total volume, green propellant if possible, low cost, commercially available if possible. The best compromise found is the thruster assembly *MR-106L 22N* from Aerojet Rocketdyne [33] with its main characteristics shown in table 2.

Figure 21: Thruster assembly *MR-106L 22N* from Aerojet Rocketdyne [33]

The thruster assembly is an important part of the propulsion system, but the whole propulsion system has to be designed, including all the fluid elements. The fuel flow

Thrust range (N)	10-34 (qualified for 40)
Minimum impulse bit (N.s)	0.015
Mass (kg)	0.59
Specific impulse (s)	228-235
Total length (mm)	186
TRL	9
Power needed (W)	36 (max)
Feed pressure (bar)	27.6 - 5.9
Expansion ratio	60:1
Propellant type	Hydrazine
Steady state firing (s)	4000 (single firing)

Table 2: Characteristics of interest of the thruster assembly MR-106L 22N from Aerojet Rocketdyne

and pressure need to be controlled precisely, and monopropellant is designed to work paired with a pressurant. The role of this pressurant is to apply load on the fuel to control its flow coming out of the tank.

From the literature [34] and the preliminary analysis [2], trade-offs are available for the choice of a pressurization system. For precise attitude control a system using a mechanical pressure regulator, and two different tanks for the fuel and the pressurant is more adapted. Compared to a system with only one tank for both fluids, it adds mass and complexity, but the benefit is that pressure acting on the propellant stays the same during the whole flight. This means that the exact same thrust level can be applied during the flight, which allows for more precise control in case of small thrust variations. On top of that, as the thrust stays constant, there will be enough thrust at the end of the flight when high thrust is needed for landing, which is not necessarily the case for other pressurization systems. Therefore, a regulated system with two different tanks is adopted.

These tanks then need to be chosen and sized. Multiple tank technologies exist for space propulsion, but the most commonly used for spacecraft's attitude control are bladder tanks [35]. These tanks are composed of a rigid metallic shell, with a flexible bladder. The fuel is contained in the bladder, while the pressurant applies a load on the exterior of the bladder, controlled by the pressure regulator. These tanks are simple to use, reliable, completely separate the pressurant gas from the fuel, and guarantee the availability of the propellant during the entire flight.

The tanks' size then needs to be determined. From the flight simulations in section 9, the mass of propellant needed for the flight has been set at $1.86kg$, which comes to $2.23kg$ with a 20% margin. With hydrazine under nominal conditions (temperature of

$298K$, storage pressure of $2.4MPa$), this corresponds to a volume of $2.18L$. The volume of pressurant needed for such a system is found in appendix E [36]. These calculations concluded that $0.945L$ of helium is needed, which corresponds to $0.154kg$ at a storage pressure of $14MPa$. The minimum mass calculated for both tanks is $0.2412kg$ for the hydrazine tank and $0.4762kg$ for the helium one. This corresponds to rules of thumb given for tank sizing [19], which gives a mass of the fuel tank of around 20% of the fuel mass. Nevertheless, it was decided to look for commercially available tanks, which contain all the additional needed elements, in particular the diaphragm for the fuel tank. The two selected tanks are designed for microsat propulsion systems. For the propellant, the *oblate spheroid rolling diaphragm tank* from MOOG [37] is chosen with a volume of $3.35L$ and a mass of $0.91kg$. For the pressurant, the *T-800 Pressurant Tank* from Infinite Composites technologies [38] is used, which has a volume of $1.4L$ and a mass of $0.4kg$. These tanks can be used to store the fuel at $2.4MPa$ and the pressurant at $14MPa$.

The final elements that need to be sized are the fuel lines. First, the total length of these lines is estimated from the configuration in section 7. With a 50% margin, as the design is still likely to move, the total length is fixed at $3.75m$.

In cubesat or smallsat missions, with similar propulsion systems [39], the diameter of the fuel elements is $\frac{1}{4}\,in = 6.36mm$, with a thickness of $0.032in = 0.81mm$ [36]. The typical material used is titanium with a density of $4500kg.m^{-3}$, which gives a total mass of $0.24kg$ for the fuel lines.

The overall design of the propulsion subsystem is based on monopropellant existing systems for main propulsion and control, such as the *Deep space one reaction control system* [40] and *GPIM system* from Aerojet Rocketdyne [41]. The drone's propulsion system diagram is shown in figure 22.

All the components used in the propulsion subsystem, with their references, are listed below, their mass and power needs being listed in the system sizing section (5.5).

- Fuel tank (x1): Moog Rolling diaphragm 7.6 inches diameter
- Pressurant tank (x1): Infinite Composites 1.4 liters T-800 Pressurant tank
- Pressure regulator (x1): Stanford MU chemical propulsion system miniature pressure regulator
- Latch valve (x1): Marotta MV602L Latch solenoid valve
- Fill and drain valve (x2): MOOG Low Pressure Titanium service valve
- Valve heaters (x4): Thermocoax electrical heating systems

- Tank heaters (x2): Epec polyimide flexible heaters
- Propellant filter (x1): MOTT Propellant filter
- Pressure transducer (x2): Paine Miniature-Satellite Series Pressure Transmitter
- Temperature transducer (x2): IST Platinium sensor
- Thruster assembly (x4): Aerojet Rocketdyne MR-106L 22N
- Fuel lines

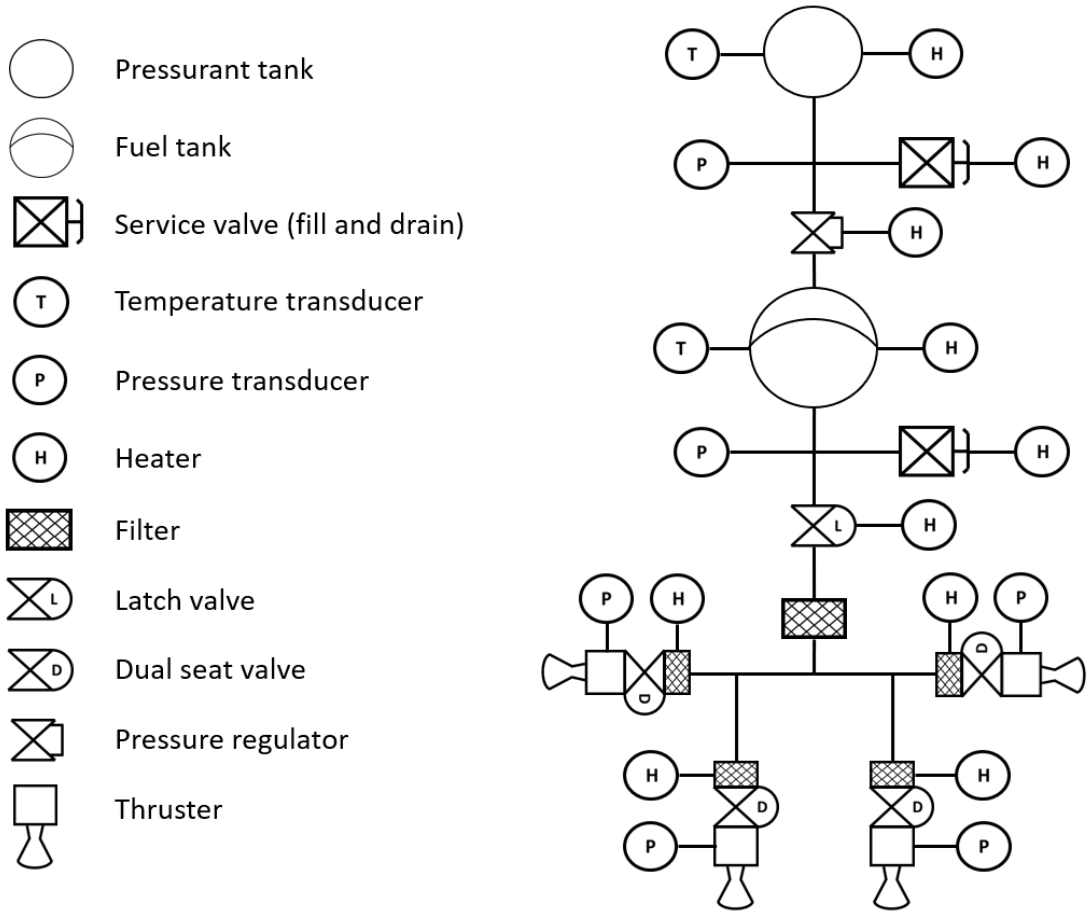

Figure 22: Simplified diagram of the propulsion system

8.2.2 Mapping instrument

During the preliminary analysis, a study was made to choose the best mapping technology for the mission's needs and requirements [2]. A trade-off was made between different methods, such as optical camera, radar, Lidar, flash Lidar, or thermal mapping. It was determined that flash Lidar is the most suitable for this application, mainly for its high resolution, 3D mapping capability, usability in a moving environment, and no need for additional moving mechanism.

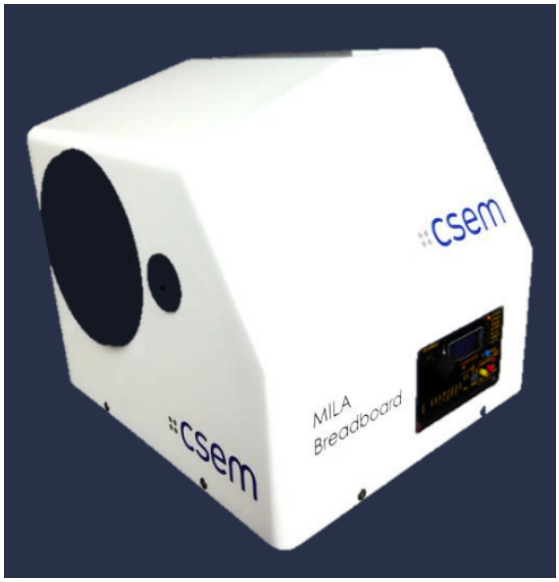

Figure 23: CSEM's MILA BB Flash Lidar

A flash Lidar emits flashes of light with a diverging laser beam on the surfaces to map. The light is reflected by the surface back to the sensor and a 3D map is created from the collected data [42]. In comparison, a standard Lidar uses a single-point laser and creates a point-by-point map, requiring moving parts. A flash Lidar then allows for a high global sampling rate as it scans the whole field of view for each measurement.

A program was initiated by ESA to develop lightweight miniature flash Lidars for future space exploration [43]. The requirements formulated by ESA are used to model the flash Lidar in this analysis: maximum allowable volume of $25cm$ x $30cm$ x $25cm$, maximum mass of $4kg$, and maximum power consumption of $35W$. The design of the flash Lidar is based on the *MILA BB* from CSEM [44][45] which follows ESA's volume and power requirement, and with a mass objective of less than $2kg$.

For the 3D configuration (section 7), it is assumed that the optical instrument can be separated from the electronic components to have a more compact overall design, and better mass distribution.

For the drone, the flash Lidar is used to obtain the mapping data, with the heavy computation done outside the drone, by the service station's OBC after the flight. But it is also used instantaneously during the flight, both for hazard detection and collision avoidance, but also to detect the landing pad during the landing. As mentioned in the previous subsection, tracking lights shall be placed on the service station to facilitate the landing.

This choice of the mapping instruments has implications for the flight strategy. Calculations showed that with this flash Lidar, the drone shall fly at a constant altitude of around $50m$ above ground level to meet the resolution requirements [2]. The maximum flight speed is $30m.s^{-1}$.

8.2.3 Electrical power system

The power budget introduced in section 5.5.2 has direct influence on the choice and sizing of the power system. The predicted maximum peak power consumption is 324W. The flight simulations (section 9) predict a nominal flight time of $120.4s$, over which a margin of 50% can be added, which gives a flight time of around $180s$ for the design of the batteries.

Figure 24: *iEPS Electrical Power System* from ISISpace, with the battery pack

From Muriel Richard's lecture on electrical power system [46], as the requirements impose around 10 battery charge/discharge cycles, the depth of discharge (DoD) can be estimated at 90% to keep the batteries operating in good conditions.

As the drone's power system's size and requirements are similar to CubeSats', com-

mercially available parts are considered. *iEPS Electrical Power System* from ISISpace is selected for its low mass, low volume, modular battery pack, and flight heritage [47]. Its efficiency η is 85 to 95 %.

The battery capacity needed can be estimated as:

$$C = \frac{P \cdot t}{DoD \cdot \eta} = 21.11Wh$$

ISISpace's Lithium-ion battery pack of 22.5Wh is then selected to complete the electrical power subsystem

8.2.4 Avionics

In this subsection, the avionics refer to all the electronic control components and sensors needed on the drone.

Figure 25: ISISpace's onboard computer

As mentioned in section 5.3, centralized data architecture is chosen, for its reliability. All the information transits through the onboard computer (OBC), which is the central part of the drone in the data aspect. It controls all the active components of the drone, and receives housekeeping data, from pressure or temperature transducers.

The OBC is also used to store the mapping data gathered by the flash Lidar. However, as seen in the previous subsection, as the instrument is still in the development phase, as the amount of data gathered is still unknown, the OBC's memory size must therefore be as high as possible in this preliminary study. The OBC's needs are also similar to CubeSat missions, so off-the-shelf components are considered. ISISpace OBC

is selected for its combination of very low weight and power consumption while having a high storage capacity (up to 32gb if needed).

With this architecture, the OBC controls every part of the drone, and all the information must transit by it. The possibility of having a separate control board for the propulsion was discussed and will have to be evaluated in the future phases of the project. The benefit of this solution is to directly know, in case of a problem during the testing phase, that it is associated with the propulsion subsystem. In this case, only that board can be removed for troubleshooting. However, this board may be present only for the testing phase and the propulsion system's operations could go back to the OBC, with a fully centralized architecture, during operations, where it is the most reliable solution.

Figure 26: Safran's *STIM377H* inertial measurement unit

While the attitude control will directly be operated by the propulsion system, a solution to measure the attitude and the position of the drone is still needed. The altitude can be directly extracted from the flash Lidar's measurements, but the yaw, pitch, roll angles and their variations, as well as the x,y position, velocity, and acceleration, need to be known during the flight. The inertial measurement unit (IMU) *STIM377H* from Safran is selected for its precision, reliability, and mass. It contains 3 highly accurate microelectromechanical gyroscopes, 3 high stability accelerometers, and 3 inclinometers, to be able to have constant knowledge of the position, velocity, acceleration, and attitude of the drone.

The pressure transducer selected is Emerson's *Paine 212-Miniature-Satellite-DS*, and the temperature transducer is *300 Series Platinum sensor* from Innovative Sensor Technology. These two components are reliable, simple, and commonly used transducers

for space application.

8.2.5 Thermal control

The thermal requirements for all the selected components are listed in table 3.

Subsystem	Component	Operating temperature range (°C)
Propulsion	Fuel and pressurant	[+8; +53]
	Pressure regulator	[-65; +85]
	Latch valve	[-25; +50]
	Fill and drain valve	[-7.2; +60]
	Propellant filter	[-73; +371]
	Temperature transducer	[-200; +300]
	Pressure transducer	[-40; +60]
Payload	Flash Lidar*	TBD
Telecommunication	Antenna*	[-40; +85]
	Transceiver*	[-40; +85]
Avionics	OBC*	[-25; +65]
	IMU*	[-40; +85]
Power	EPS + battery pack*	[-20; +70]
Thermal control	Flexible heaters*	[-195; +200]

Table 3: Operating temperatures for the selected components

Note that the fuel and pressurant must be at the same temperature to avoid thermal loads, and for the control to be as precise as possible during flight, they have therefore the same operating temperatures.

In the table, the components with an asterisk are inside the warm electronic box, which contains all the sensitive electronic components, with similar thermal requirements. It will also need less power to maintain all the components in their operating range.

To maintain the drone in its operating temperature, active electrical heaters are used, such as *Polyimide / Kapton Flexible Heaters* from Epec, which heat the electronic box when flying in the PSRs where the external temperature is extremely low.

The active components of the propulsion systems such as the valves or the pressure regulator will need to be heated in the same way, as well as the propellant and pressurant tanks, to prevent the hydrazine to freeze. Finally, heaters are included in the thrusters assemblies, mainly to heat the catalyst bed, to be able to provide thrust during the flight. As shown in the preliminary analysis [2], one big challenge is to control the passive components' properties such as the heat capacities, emissivity, or absorptivity, to stay within all the components' operating range, while consuming the least possible

power. To do so, precise thermal simulations, based on the 3D configuration from section 7 will be required to fix the material used, mainly for the exterior panels. Multilayer insulation for the external surface and thermal straps inside the drone to distribute the heat will also have to be considered in the design when the results from the thermal simulations will be known.

8.2.6 Telecommunication

The communication during the flight was previously considered [2]. But the drone shall be completely autonomous. If there is a problem during the flight, the drone shall be able to solve it internally. And even if there is communication between the drone and the base, the service station won't have more capability to solve the problem than the drone itself. There is then no need to have communication during the flight, everything can be transmitted with wires, once on the service station.

However, at this stage of the project, a wireless communication system can be kept for redundancy with wired communication. Indeed, if there is a problem with the downlink of the data (for example, dust impeding the power interface), this wireless system can be used. For CubeSat or smallsat, this type of communication is typically made with UHF bands, at a low data rate [48][49]. This is not a problem in this case, indeed, the amount of generated data can be high, but the time to transmit it is very long, as the interval between two flights is also very long. The need for such a wireless communication system will have to be re-evaluated in the future phases.

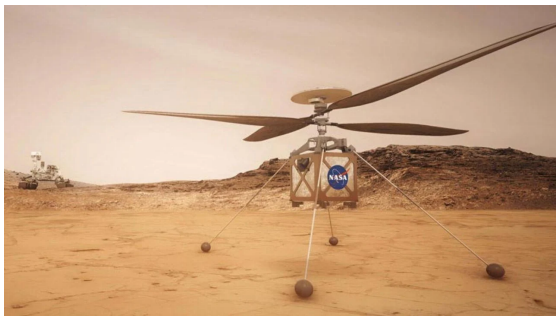

Figure 27: Artist view of NASA's ingenuity helicopter, with its telecommunication system on the top

The estimated needs for the drone, in terms of data rate and range, are similar to the ingenuity helicopter ones. For ingenuity, the data transfer is made using radio communication with UHF radio and a commercial Zigbee antenna at 900 MHz, with a data rate of 20 to 200 kbps [50].

CubeSat parts can be used for the UHF transceiver, and the *CubeSat UHF Digital Radio Transceiver SatCOM UHF* from Nanoavionics is selected. Its data rate is small compared to other CubeSat transceivers, but it is extremely light with only 7.5 grams.

8.2.7 Structure and wiring

The structure of the drone is designed to hold all the components. It needs to resist vibrations and small impacts. All the fluid elements, such as the thrusters, the tanks, or the different valves are attached to the structure, as well as the warm electronic box. The preliminary design of the structure is shown in section 7.

Structure and wiring are two components of the drone that are complicated to size during such early phases of the project, especially to determine their masses. However, some statistics from the literature can be used. Structure takes typically 10 to 20% of the dry mass for already existing spacecraft with propulsion systems [51][52]. This leads to an estimation of 1.5 to 2kg for the drone's structure The wiring, weighs typically around 4% of the dry mass of spacecrafts [52], which corresponds to a value of around 0.6kg in the mass budget.

Structural calculations have been made, based on ingenuity's requirements [50]. The drone's trajectory is designed to provide a soft landing, but the same strategy as ingenuity is adopted, namely, if there is a problem, the drone shall resist a fall of 0.5m. A model of this impact during landing has been made, with the details of the calculations in appendix F.

9 Flight simulation and optimization

9.1 Introduction

For this feasibility analysis, the main goal of this section is to have a good approximation of the fuel consumption, flight time, and trajectory of the drone. For any space mission, mass is one of the key drivers, and for this mission, with these requirements, it can be even more important as the propulsion is one of the key and critical aspects of the mission. If the mass consumption is too important to fit the exploration environment, the drone could be heavier than the mass requirement and should have big propellant tanks that could not allow it to fit inside the service station.

The main requirements for the flight are the following:

- The drone shall be able to take off, fly 400m and come back. (This requirement, formulated last semester [2] with margin added, comes from the Viper Rover's mission objectives, which has to drive 200m inside the PSR [53])
- The flight altitude must be constant at around 50m ($\pm$1m), with a maximum flight speed of 30m/s. (Comes from Lidar calculations [2])

Flexibility on the flight trajectory must be considered, keeping in mind the most important design aspects which are fuel consumption, flight time, and reliability, especially for the landing, which is the most critical phase. Other limiting factors will be introduced later in this section.

As explained earlier, in the propulsion subsystem section (8.2.1), a choice has been made to only have thrusters to control the whole satellite. In this approach, the vertical movement is obtained when every thruster is providing the same thrust. Then to be able to move horizontally, a differential thrust is provided, which increases the pitch angle, which is then kept stable. At this stage, the thrust is constant from the four thrusters, a horizontal force component is created which enables the horizontal acceleration. The trade-off between this method and a system with independent thrusters for vertical and horizontal movement is shown in appendix C.

The result of the trade-off is that the second solution can have a slightly lower fuel consumption because there are no fuel losses due to the angle of the thrusters (as explained later in subsection 9.6). However, the main problem with this solution is that there is no pitch, yaw, or roll control. Without this, the drone can become unstable with small external perturbation. With this solution, some other ways to avoid instability must be added, such as additional thrusters or momentum wheels. The systems would become much heavier, larger, and more complex. The first described solution with only four thrusters is then kept for flight control.

9.2 Model

A flight simulation was developed using a Simulink code. This model's main goal is to determine the flight trajectory and flight parameters such as velocity, angles, etc., but also the fuel consumption or the flight time. Note that the complete model is available in the appendix G. The preliminary optimal flight trajectory, and behavior of the drone during flight, are obtained under the following assumptions:

- 2D simulation
- Homogeneous mass distribution
- Thrusters modeled as controllable force vectors
- Constant mass
- No fuel losses
- Thruster step response modeled as a ramp of 80 ms

Note that no information is available on the step response for the specific thruster used, but for the $MR-80B$ coming from the same manufacturer and the same series, the step response is approximately 80ms [54]. This value is then used for the step response of the drone's thrusters.

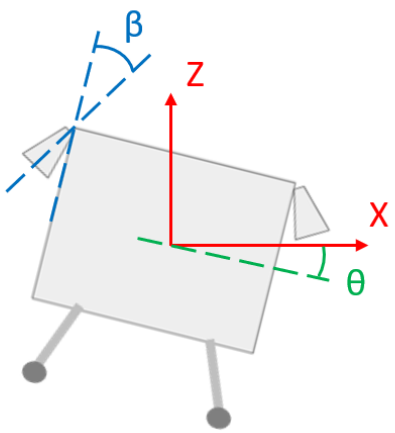

Figure 28: 2D model of the drone used in the simulation, with the pitch angle θ and the thruster angle β

The input parameters of the simulation are the mass, the 2D geometry of the drone, the thrusters' performances (specific impulse), the placement of the thrusters and their

angle β (as shown in figure 28), and how much thrust is delivered by each thruster as a function of time.

With all these parameters, the most relevant data obtained contains the position, velocity, and acceleration along the X and Y axis, the pitch angle θ of the drone (see figure 28), the flight time, and the fuel consumption.

In this model, the force delivered by each thruster is the main parameter that can be tweaked to obtain different flight trajectories. Three of them were simulated: ballistic trajectory, vertical take-off and landing with horizontal hovering, and semi ballistic with horizontal hovering. The best approach was determined using a trade-off.

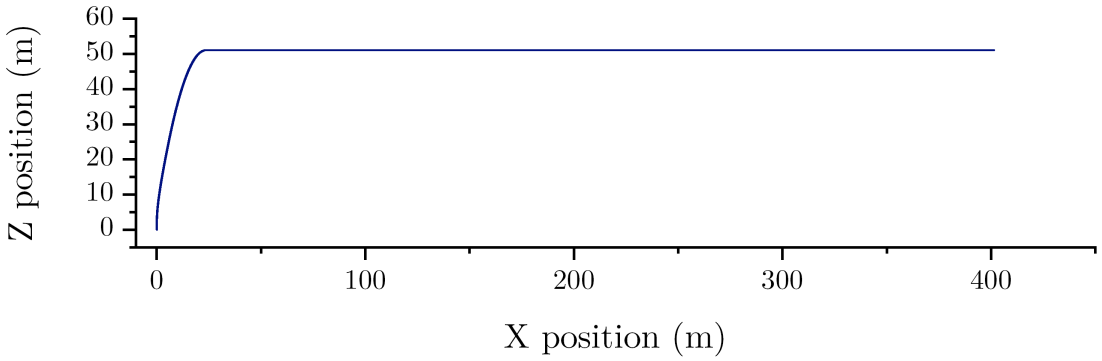

Figure 29: Symmetric semi-ballistic trajectory

The result of this trade-off is that the ballistic trajectory has the lower fuel consumption but cannot be kept, mainly because of the too high altitude variation during flight (+ 200m AGL after 400m of flight), which does not respect the requirements. On top of that, the landing is very hard to control, as the thrusters' burns are made very far from the landing pad, and in real situations, major corrections will be needed which will consume much more fuel.

The completely vertical take-off and landing option presents higher fuel consumption, and a longer flight time, but it is very easy to control and will have a very safe landing, as the drone will have the time to check if the placement is good before initiating the landing maneuver.

Finally, the semi-ballistic is a mix of the two previous trajectories. The take-off is vertical for the first few meters, then a ballistic trajectory is initiated up to the altitude of 50m. When the drone reaches this altitude, it is kept constant, and with a constant horizontal acceleration. The trajectory is fully symmetric, with, as for the take-off, the last few meters fully vertical before landing. This provides good safety, as small corrections can easily be made in the last vertical phase above the landing pad. Using this trajectory, the fuel consumption is 13.1% lower than the completely vertical/horizontal if all the other parameters are kept unchanged.

The trajectory obtained with this semi-ballistic trajectory is shown in figure 29. Note that the trajectory is completely symmetric, with the drone turning around after 400 meters.

All the steps necessary for this trajectory are simplified and represented in figure 30.

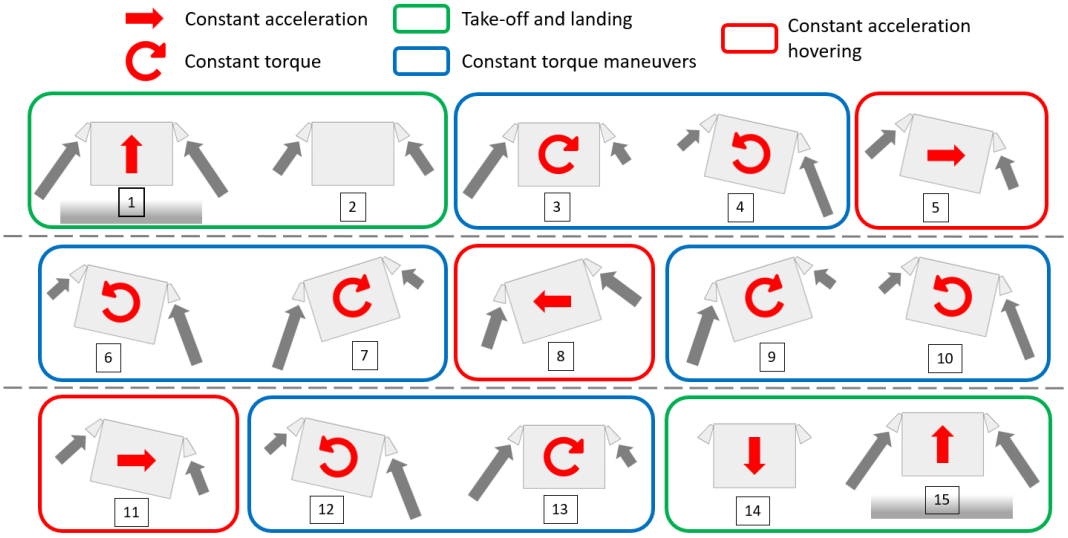

Figure 30: Thrust strategy required for the semi-ballistic trajectory

9.3 Example

To better understand the model, an example is introduced in this subsection, with the corresponding results.

The following example models the semi-ballistic trajectory introduced in the last subsection (see figure 29 for the resulting trajectory). The input parameters used are a mass of $15kg$, a 2D cross-section of $0.5m$ x $0.5m$, and the thrusters placed on the top corners of the drone, with a thruster angle of 45°. Figure 31 shows the thrust delivered by the two back thrusters (in yellow) and the front ones (in blue).

Figure 31 shows a slightly different thrust, coming from the back and front thrusters, during a few phases of the flight. These differential thrust phases allow for maneuvers to modify the pitch angle of the drone and stabilize it, as seen in figure 32a. This provides a force in the horizontal direction while keeping the vertical acceleration zero to keep a constant altitude, as shown in figures 32b and 32c. The fuel consumption during the flight for this example is also shown in figure 32d. Note that all the figures derived from this example are available in the appendix H

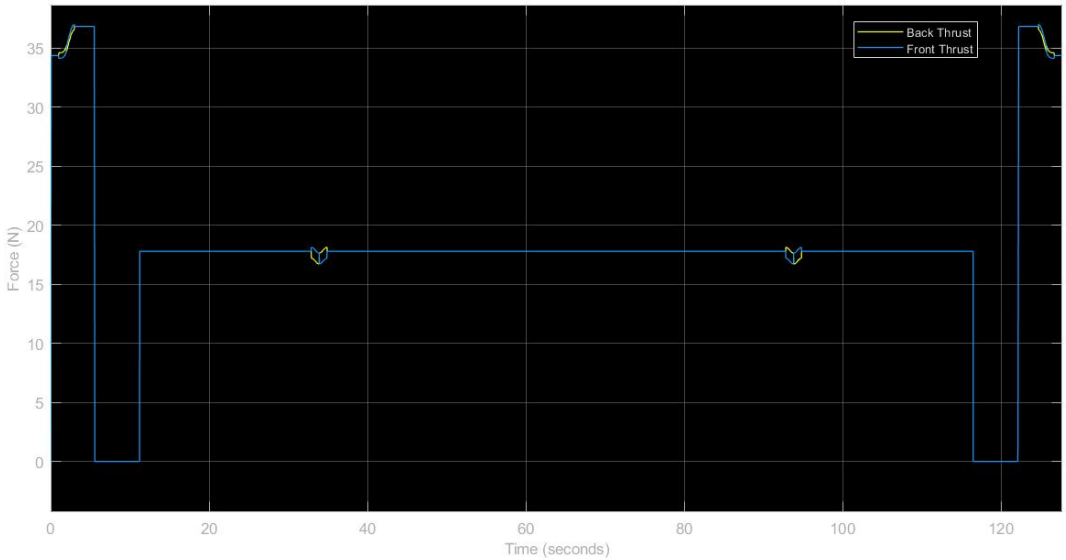

Figure 31: Thrust provided by the back and front set of thrusters to obtain a semi-ballistic trajectory for this example. (During most of the flight, the blue and yellow curves are superimposed

In figure 31, the sudden thrust changes are modeled with ramps, such that the thruster can go from $0N$ to the maximum thrust in $80ms$. Note that the thrusters must be able to be controlled finely, with small thrust variations: impulses of $0.08N.s$, the thrusters minimum impulse bit must then be chosen accordingly, as said in section 8.2.1.

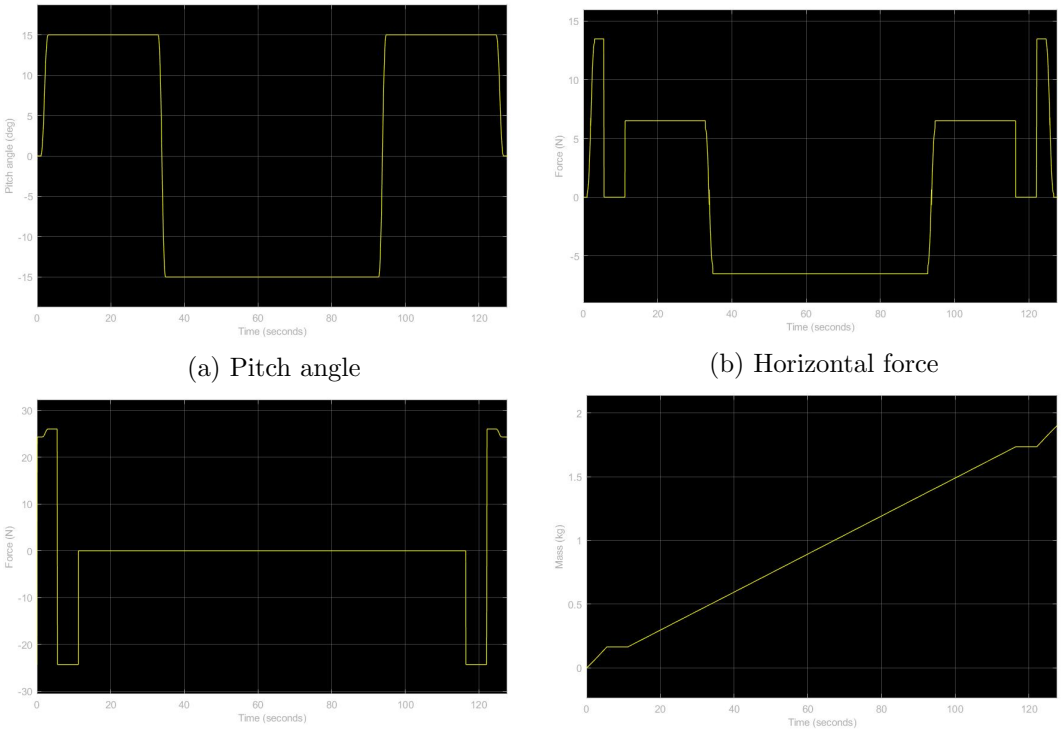

(a) Pitch angle

(b) Horizontal force

(c) Vertical force

(d) Fuel consumption

Figure 32: Results of the example introduced in section 9.3, for the semi-ballistic model

9.4 Results

Several simulations were made with different input parameters to see what is the effect on the flight parameters. For these simulations, the main goal was to minimize fuel consumption and flight time. As justified in subsection 9.2, the simulations are made with a semi-ballistic trajectory, with a mass of $15kg$, and a square cross-section of $0.5m$ x $0.5m$.

Two main parameters are studied to analyze their influence on the flight, and mainly on the fuel consumption and flight time: the thruster angle and the pitch angle.

Thruster angle: A first set of simulations is presented, which was made with a fixed pitch angle of 15° and a variable thruster angle. The fuel consumption is shown in figure 33.

Using this model, the lower the thruster angle is, the lower the fuel consumption is. This is due to the fact that if the thrusters are almost vertical, the losses due to the horizontal component of the thrust, coming from the front and back thrusters during

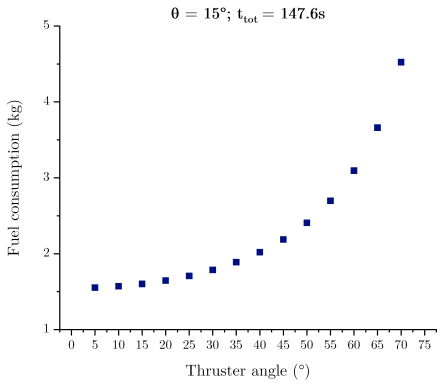

Figure 33: Fuel consumption with respect to the thruster angle. The pitch angle is fixed at 15° and the obtained flight time is 147.6s

the hovering phases, are minimal. As shown in figure 34, in this situation, the majority of the force provided by the thrusters is used to maintain the altitude, and accelerate horizontally.

On the other hand, if the thruster angle is high, the thrust vectors are more oriented towards the x-axis of the drone. Then a lot of force generated by the back thrusters is compensated by the front ones, and the vertical component is lower with the same thrust level provided by the thrusters. Therefore, to maintain a constant altitude, more thrust is needed, and more fuel is consumed.

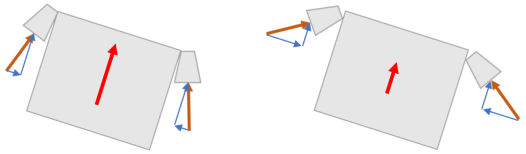

Figure 34: Total force (in red) provided by different thruster angles

Note that, as explained, the thruster angle has a direct implication on fuel consumption. But as more fuel is consumed, the sum of forces applied to the drone is the same, therefore, the thruster angle does not influence the flight time.

Pitch angle: Here, the thruster angle is kept constant at 45°, while the pitch angle varies. The results for the fuel consumption and the flight time are shown in figures 35a and 35b. These results show that a high pitch angle leads to low fuel consumption. This is mainly because, as seen in figure 34, the higher the pitch angle is, the more horizontal is the force vector. To maintain a constant altitude, the thrust then needs to be higher,

as the horizontal component decreases with the pitch angle, increasing the instantaneous fuel consumption. But on the other side, with more horizontal force, the acceleration and velocity of the drone are much higher, the hovering phases are then much shorter, as well as the total flight time. Consequently, even with higher instantaneous fuel consumption, with the flight time being shorter, the total fuel consumption is lower.

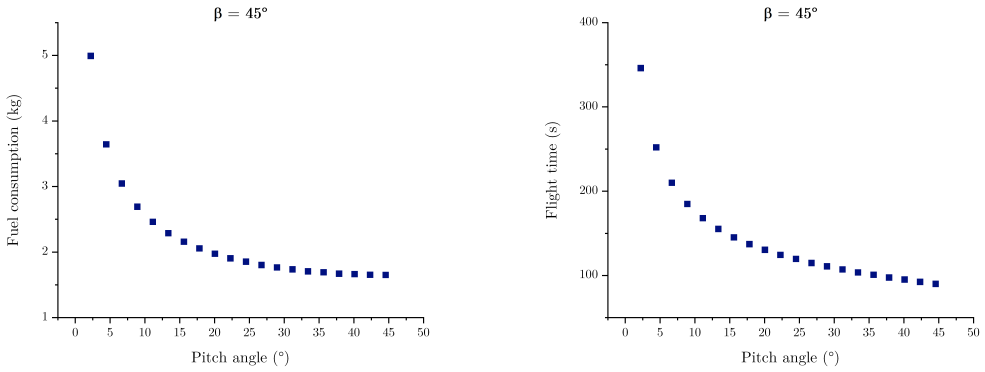

(a) Fuel consumtion

(b) Flight time

Figure 35: Fuel consumption and flight time with respect to the pitch angle, with a constant pitch angle of 45°

9.5 Pitch angle optimization

In the previous subsection, it was shown that to minimize fuel consumption and flight time, the pitch angle has to be as high as possible. However, a high pitch angle can lead to problems for other subsystems.

The flash Lidar both needs to make measurements for mapping and also to see the surroundings for collision avoidance. The flash Lidar must therefore be able to map what is vertically underneath the drone. As the field of view of the CSEM's flash Lidar, used as a reference in this analysis, is not yet known, other flash Lidars are used for this value. NASA's *3-Dimensional Imaging Flash Lidar* is expected to have a wide field of view of 24° [55], which is kept for this preliminary analysis.

Two options were considered to deal with this limitation: keep a pitch angle lower than 24°, or attach the flash Lidar to a mechanical gimbal. A trade-off was made between these solutions. If a gimbal is used, it is assumed that the drone can fly with a pitch angle as high as 45°, and stay in the flash Lidar's field of view requirements.

Then flight simulations were made, using the same inputs parameters as in section 9.4. With a pitch angle of 45°, which corresponds to the solution with the gimbal, the fuel consumption for one flight is $1.6482kg$, and the flight time $89.4s$. For the other

method, with a pitch angle of 24°, the fuel consumption is $1.8602kg$ with a flight time of $120.4s$.

There is a significant difference in flight time (-26%), but the fuel save is less important (-11%). However, from NASA's under development gimbals for space application [56], it can be assumed that to support a $2kg$ flash Lidar, the gimbal's weight will be in the order of magnitude of $0.5kg$. Taking into account the added mass of the gimbal in the flight simulation, the fuel saved with the gimbal solution drops to $132g$ which corresponds to 7%.

Given the added complexity of the gimbal system, with additional moving parts which are very critical in the dusty lunar environment, it was decided that the fuel save was too low compared to the potential failure added that can endanger the mission, so the solution to limit the pitch angle at 24° is kept.

However, this solution must be kept in consideration for the next phases of the mission. Indeed, when a detailed thermal analysis will be made, if it is determined that the flight time has to be extremely low to avoid over/underheating during the flight, this gimbal solution can be assessed.

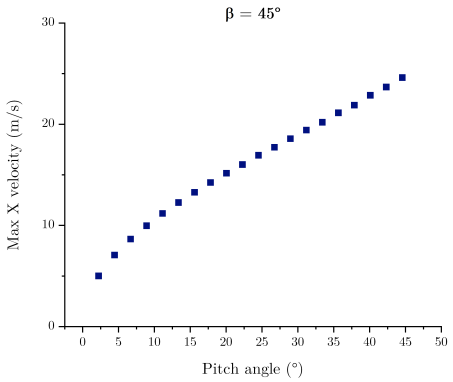

Figure 36: Maximum horizontal velocity for different pitch angles

The maximum velocity as a function of the pitch angle is shown in figure 36. The speed corresponding to pitch angles of 24° and 45° are respectively $16.68m/s$ and $24.75m/s$, which respect the requirements for the maximum flight velocity of $30m/s$.

9.6 Thruster angle optimization

It was shown in subsection 9.4, that to minimize fuel consumption, the thruster angle shall be as low as possible. This means that the thrusters must be as vertically oriented as possible. In this case, new limitations come from other subsystems. The thrusters

exhaust hydrazine at a very high temperature and with a very high velocity. This leads to three main problems: dust dispersion, damaging and heating of the structure, and disturbance for the optical measurements (if the exhaust gas goes in the field of view of the Flash Lidar, then the light emitted and reflected will travel through the gas instead of vacuum at a different speed, hence decreasing the accuracy of the measurement).

Therefore, the goal of this subsection is to visualize the exhaust gas coming out of the thrusters in operating conditions, to mitigate the three aforementioned aspects.

To do so, fluid simulations of the thrusters were made. First, the 2D geometry of the thruster is defined in figure 37, from the dimensions of the thrusters [33].

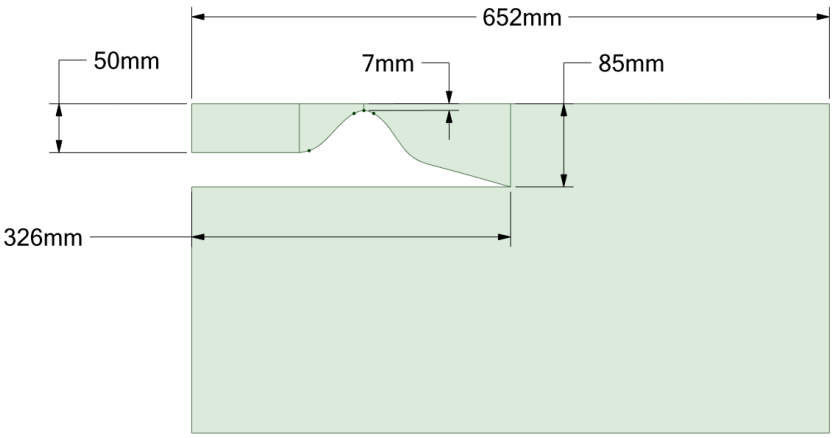

Figure 37: 2D geometry used in the fluid simulations

The model used for the fluid simulations contains the following assumptions [57][58][59].

- Steady-state, 2D axisymmetric model
- $k - \epsilon$ turbulence model with compressibility effects
- Operating pressure: 0Pa
- Compressible fluid
- Density modeled with ideal gas law
- Boundary conditions: Thruster pressure inlet: 2.4MPa, Far field conditions: Pressure outlet with gauge pressure: 0Pa, No-slip condition with the thruster's wall
- Pressure-velocity relation: Coupled with Rhie-Chow Distance Based solver

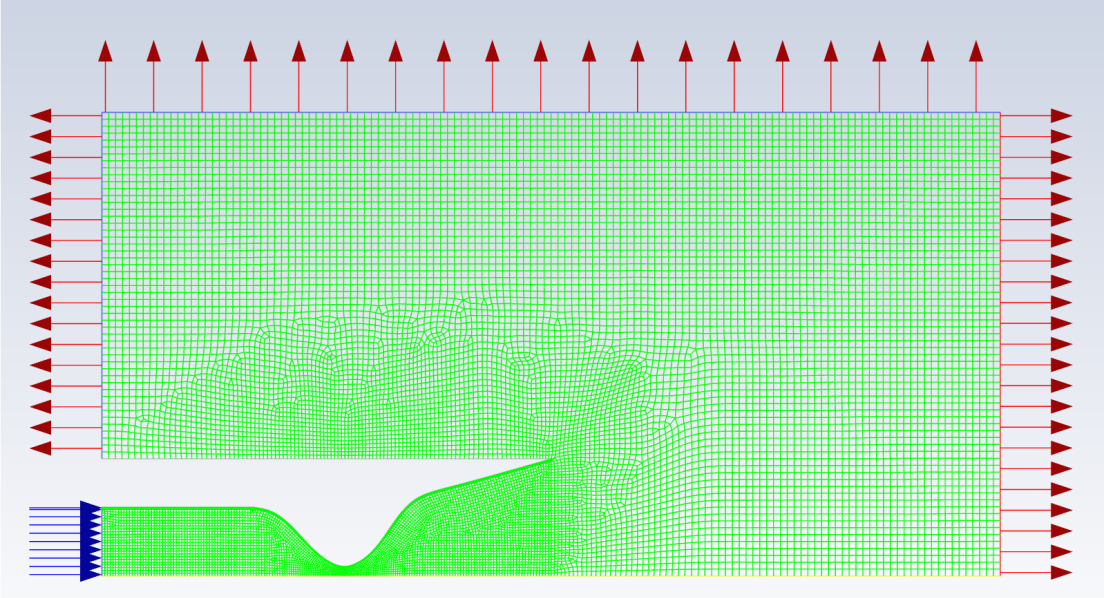

Figure 38: 2D geometry used in the fluid simulations, with the corresponding mesh and boundary conditions

Figure 38 shows the geometry used with the corresponding mesh and the boundary conditions.

Note that as these simulations are for visualization purposes to understand the behavior of the exhaust gas, and not to derive quantitative values, air following the ideal-gas law is used as the working fluid.

The streamlines obtained from this model are shown in figure 39. At steady state, they follow the trajectory of the gas particles in the thruster. As the inlet is at very high pressure, with near-vacuum in the far field, the flow stabilizes at a constant velocity in the first part of the nozzle, then accelerates in the converging part. The flow is choked at the throat of the nozzle, where the transition to supersonic speeds happens. In the diverging part, the flow is further accelerated, before keeping a close-to-constant velocity behind the nozzle.

Two regions are visible in the streamlines, and in the pressure field shown in figure 40. The first one in the center, behind the nozzle, contains fluid at high speed and very high pressure. This zone can make a lot of damage to the structure, as well as dust dispersion. However, this zone has a very narrow-angle, and these problems can be mitigated by increasing a little the thruster angle.

But a second zone is visible in the streamlines and temperature field (figure 41). This zone is less dangerous than the previous one because its pressure is much lower, but the

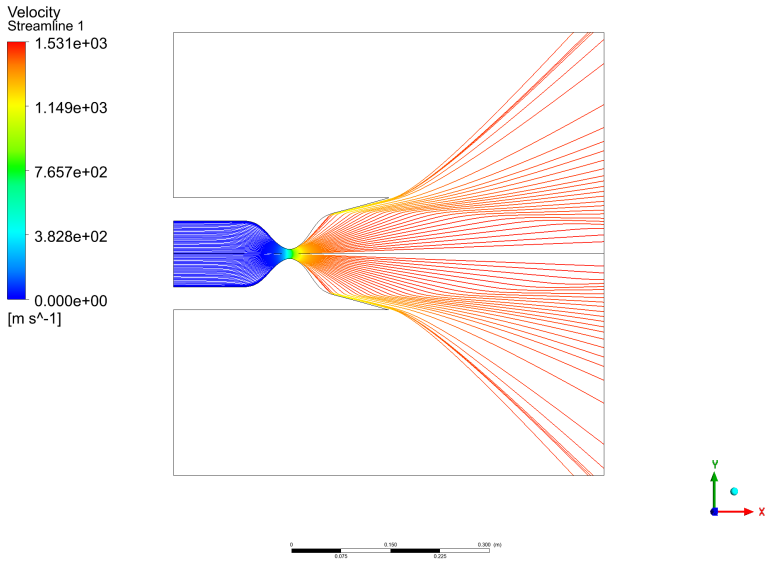

Figure 39: Streamlines coming out of the thrusters, colored with the velocity

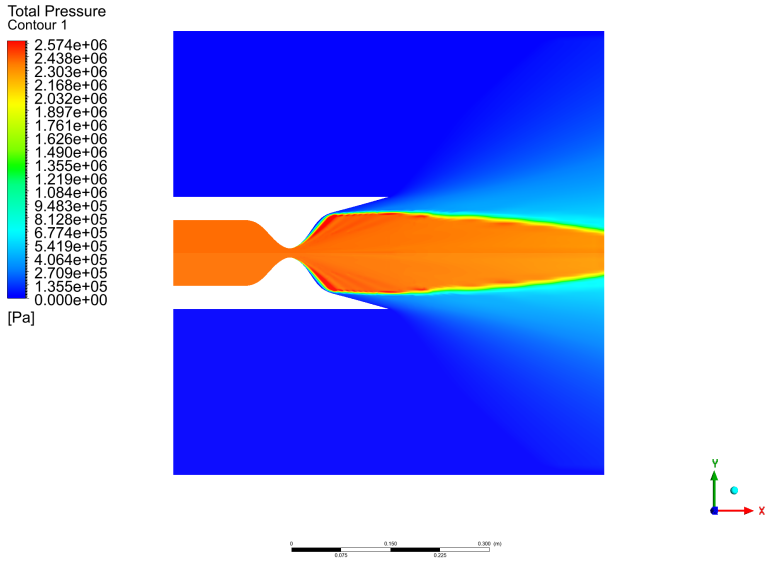

Figure 40: Total pressure field

temperature is still very high and can damage the structure. Behind the thruster, this region has a much wider angle, at around 38°. This zone is the main limiting factor for the thruster angle. To avoid dust dispersion, measurement disturbance, heating, and damage to the structure, the thrusters shall then be placed at an angle higher than

these 38°. Therefore, an angle of 45° is defined as the minimum admissible thruster angle, taking 20% of margin.

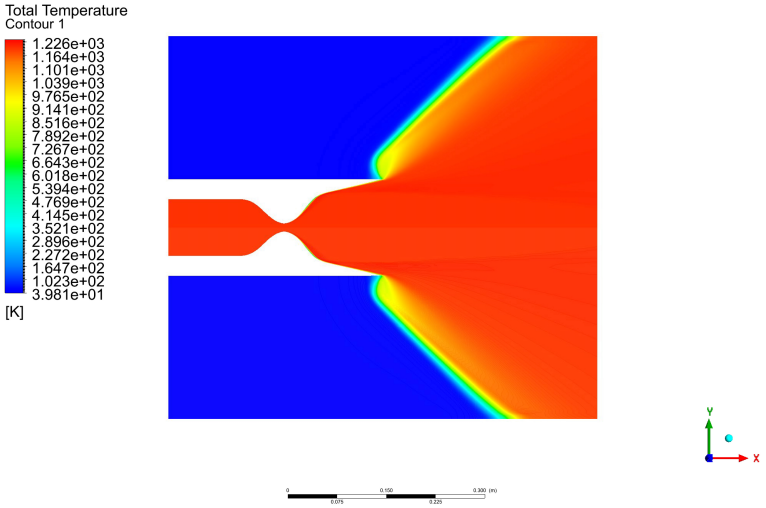

Figure 41: Total temperature field

With this thruster angle of 45°, the fuel consumption is 28% higher than if they are fully vertical, but this is necessary to mitigate all the potential failures mentioned previously.

9.7 Optimal flight conditions

The analysis carried out in this section led to the definition of optimal flight conditions that meet all the requirements, and all the design limitations. These values are used throughout this thesis:

- Fuel consumption: $1.86kg$
- Flight time: $120.4s$
- Maximum horizontal velocity: $16.68m/s$
- Thruster angle: 45°
- Pitch angle: 24°

10 Conclusion and future work

I will start this conclusion by saying that it was a pleasure to be working on this thesis all along this semester. It was a privilege to be part of such an ambitious project, and I am more than happy I could contribute to its advancement.

But more specifically regarding the work made this semester, even if some things could have been done better (which will be discussed later in this section), I am globally very satisfied with the progress made along this Master's thesis. As the project already started last semester, and I was not familiar with lunar missions and the lunar environment, especially permanently shadowed regions, I started by spending several weeks gathering information on these subjects, as well as reading in great detail all the documentation available on the project. At that time I was frustrated not to start working on new material, but looking back I am now convinced that all this time was fundamental. Indeed, this allowed me to have a deep understanding on what were the challenges of this mission, and how to tackle them efficiently.

The organization of the work through the semester, with autonomous work on my side, and long weekly review and discussion sessions with David Rodriguez was efficient, and I think was the way to go. On top of that, the fact that he was always available to answer my questions and doubts helped me a lot.

However, it would have been beneficial to have someone else working on a different aspect of the project. For example, it would have been interesting to work with someone focusing on the mapping, or the control algorithm. With someone working on areas out of my field of expertise, or on subjects on which I couldn't go deep, being constrained by the 4 months of a Master's project. These aspects would have been developed in detail, which could have had an impact on the design. Moreover, discussing with people with a different point of view on the project would have led to an interesting insight, and maybe a different approach to some aspects of the work.

All the objectives set at the beginning of the semester could not be met, the thermal analysis, and the service station's system level design especially. If some of these aspects could have been tackled with a different schedule, I nevertheless think that the approach used this semester was the right one. Indeed, if the thermal analysis or the service station design were addressed, then either some other parts should have been dropped, or the work on these elements would have been very superficial. As I think the aspects addressed this semester, mainly the risk analysis, the propulsion system, the optimal flight conditions determination, or the drone design, were more critical for the feasibility analysis in this very early stage of the project, if I had to start over, I would tackle the subjects on the same order.

However, some of these subjects, which still have to be addressed, remain critical for the feasibility of the project.

The service station has to be designed, especially the interfaces between the drone and the station, but also with the rover, which was considered out of the scope of the analysis for now. As the dust dispersion is one of the most critical aspects given by the risk analysis, a deep focus will be needed on the fluid, power, and data connections, and the way to avoid dust to obstruct these interfaces. The design of the flame deflector, helped by the fluid simulations made this semester, the station's cover, and the guiding and locking mechanisms will also be important parts of the next phases.

The concept of operations was defined at the system level, it will have to be made at the subsystem level for every component of the drone. A detailed definition of the safe mode is also needed, and the same approach will have to be adopted for the service station.

Although a first thermal analysis was made last semester, the model used was very simple, due to a lack of knowledge on the design of the drone. Now that a preliminary design has been defined, with a choice and configuration of each component, the basis is set for an in-depth thermal analysis. Knowing the exact 3D configuration of the drone, with the thermal requirements for each component, precise transient thermal simulations can be made to mitigate the risk of overheating or underheating depending on the flight conditions. The inside configuration can then be adapted, as well as the external material of the drone, to optimize the thermal distribution.

This 3D design can also be used to define a proper control algorithm for the drone. A full flight simulation can be made, with the potential evaluation of different flight strategies. Off nominal flight simulations can also be done, with for example the definition of a strategy on how to land back on the base if one of the thrusters fails.

This preliminary design sets a strong basis for future work on this project. The system architecture was defined, including the requirements and the concept of operations for the drone, which are the basis for all the analysis. The design of all the subsystems, with a focus on the propulsion, allowed to obtain a precise understanding of the whole system, including its mass and power requirements. The flight simulations led us to the optimal flight trajectory, with the fuel and time needed to achieve the mission's objectives. The 3D design and configuration will also be the basis for the work that needs to be done in the future phases, especially on the thermal analysis and the flight control. Finally, the risk analysis, which was updated throughout the work, gave insight into the most critical parts of the mission, which were, for most of them, tackled this semester, or need to be addressed in the following phases of the project for the others.

In the course of this analysis, some previously unknown aspects that were considered potentially critical were tackled, and none of them led to the conclusion that the project was unfeasible.

The design was done with the objective to assist a rover mission in permanently shadowed regions on the Moon, but can however be adapted to other mission scenarios,

such as the exploration of lunar lava tubes or other celestial bodies, and paves the way for future airborne exploration in vacuum conditions.

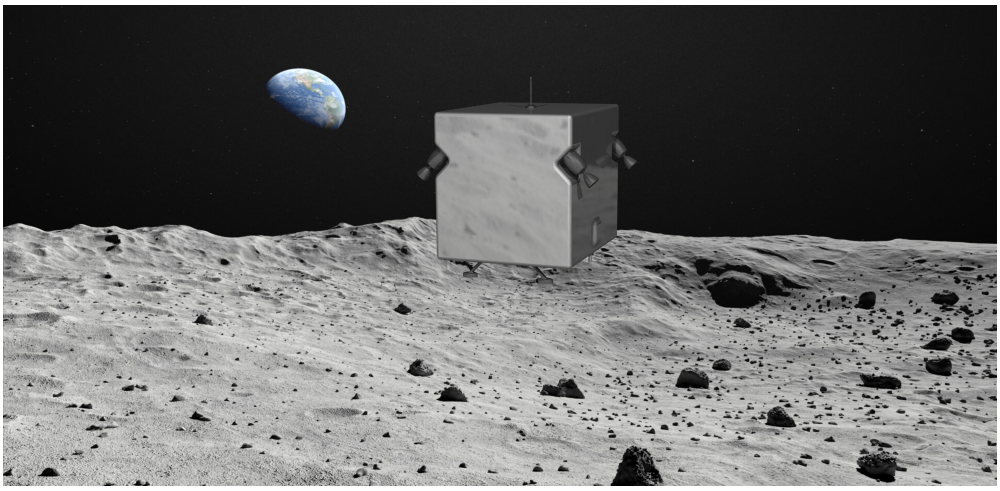

Figure 42: View of the lunar reconnaissance drone

References

[1] A. Colaprete et al. "An Overview of the Volatiles Investigating Polar Exploration Rover (VIPER) Mission". In: *AGU Fall Meeting Abstracts*. Vol. 2019. Dec. 2019, P34B-03, P34B–03.

[2] Thomas Pfeiffer and Erik Uythoven. *Preliminary Design of a Lunar Reconnaissance Drone*. EPFL Ecole Polytechnique Fédérale de Lausanne, 2021.

[3] David Rodriguez. "The Moon in a nutshell". In: *Lunar Research and Technology Development, eSpace, EPFL Space Center* (July 2021).

[4] David Beale, Daniel Harris, and Joseph Bonomett. *Lunar Engineering Handbook, ESMD Course Material : Fundamentals of Lunar and Systems Engineering for Senior Project Teams, with Application to a Lunar Excavator*. https://www.eng.auburn.edu/~dbeale/ESMDCourse/. NASA's Exploration Systems Mission Directorate (ESMD), 2021.

[5] Megan Henriksen. *Casting Light on Permanently Shadowed Regions*. http://lroc.sese.asu.edu/posts/979. NASA/GSFC/LROC, School of Earth and Space Exploration, Arizona State University, Jan. 2018.

[6] NASA National Aeronautics and Space Administration. *LUNAR RECONNAISSANCE ORBITER: Permanently Shadowed Regions on the Moon*. https://lunar.gsfc.nasa.gov/images/lithos/LRO%20litho5-shadowedFinal.pdf. Goddard Space Flight Center for NASA's Science Mission Directorate, 2013.

[7] Tetsuya Kaku et al. "Detection of intact lava tubes at Marius Hills on the Moon by SELENE (Kaguya) Lunar Radar Sounder". In: *Geophysical Research Letters* 44.20 (2017), pp. 10–155.

[8] NASA/GSFC/Arizona State University. *PIA12954: Marius Hills Pit – Lava Tube Skylight?* https://photojournal.jpl.nasa.gov/catalog/PIA12954. Jet Propulsion Laboratory, NASA, Mar. 2010.

[9] Cheryl Lynn York et al. "Lunar Lava Tube Sensing". In: *New Technologies for Lunar Resource Assessment*. Ed. by Rick C. Elphic and David S. McKay. Dec. 1992, p. 51.

[10] M. S. Robinson et al. "Lunar Reconnaissance Orbiter Camera (LROC) Instrument Overview". In: *Space Science Reviews* 150.1 (Jan. 2010), pp. 81–124. ISSN: 1572-9672. DOI: 10.1007/s11214-010-9634-2. URL: https://doi.org/10.1007/s11214-010-9634-2.

[11] V. T. Bickel et al. "Peering into lunar permanently shadowed regions with deep learning". In: *Nature Communications* 12.1 (Sept. 2021), p. 5607. ISSN: 2041-1723. DOI: 10.1038/s41467-021-25882-z. URL: https://doi.org/10.1038/s41467-021-25882-z.

[12] Arup Roy Chowdhury et al. "Orbiter High Resolution Camera onboard Chandrayaan-2 Orbiter". In: *Current Science, Vol. 118, No. 4* (Oct. 2010).

[13] M. Kato et al. "The Japanese lunar mission SELENE: Science goals and present status". In: *Advances in Space Research* 42.2 (2008), pp. 294–300. ISSN: 0273-1177. DOI: https://doi.org/10.1016/j.asr.2007.03.049. URL: https://www.sciencedirect.com/science/article/pii/S0273117707002657.

[14] M. S. Robinson and ShadowCam Team. "ShadowCam: Seeing in the Shadows". In: *Lunar Polar Volatiles*. Vol. 2087. LPI Contributions. Aug. 2018, 5028, p. 5028.

[15] Karin Valentine. *NASA funds hopper to explore lunar polar craters*. https://news.asu.edu/20210720-nasa-funds-hopper-explore-lunar-polar-craters. Arizona State University, 2021.

[16] T. Martin et al. "S. P. Hopper: First In-Situ Exploration of Lunar Polar Terrain". In: *53rd Lunar and Planetary Science Conference*. 2022. URL: https://elib.dlr.de/148673/.

[17] Alexandra Witze. "Will NASA's Moon rover find enough of the ice it seeks?" In: *Nature* (2021). DOI: 10.1038/d41586-021-02578-4.

[18] Muriel Richard and Michaël Juillard. *Lecture notes in Spacecraft Design and System Engineering, Command and Data Handling*. EPFL Space Engineering Center, 2019.

[19] James R. Wertz, David F. Everett, and Jeffery J. Puschell. *Space Mission Analysis and Design*. 1st ed. Springer Dordrecht, 1991.

[20] *Space mission engineering : the new SMAD*. eng. Space technology library ; v. 28. Hawthorne, CA: Microcosm Press, 2011. ISBN: 9781881883159.

[21] Muriel Richard. *Lecture notes in Spacecraft Design and System Engineering, Space Mission and Systems Engineering*. Space Center EPFL, 2019.

[22] "Spacecraft Systems Engineering". In: *Spacecraft Systems Engineering*. John Wiley and Sons, Ltd, 2011. ISBN: 9781119971009. DOI: https://doi.org/10.1002/9781119971009.fmatter. eprint: https://onlinelibrary.wiley.com/doi/pdf/10.1002/9781119971009.fmatter. URL: https://onlinelibrary.wiley.com/doi/abs/10.1002/9781119971009.fmatter.

[23] Melissa Jones et al. "The Use of the Expanded FMEA in Spacecraft Fault Management". In: *2018 Annual Reliability and Maintainability Symposium (RAMS)*. 2018, pp. 1–6. DOI: 10.1109/RAM.2018.8463117.

[24] Ada Kristine et al. *Implementation of FMECA in Small Satellite Development*. NTNU Norwegian University of Science, Technology Faculty of Engineering Department of Mechanical, and Industrial Engineering, 2019.

[25] Siamak Tafazoli. "A study of on-orbit spacecraft failures". In: *Acta Astronautica - ACTA ASTRONAUT* 64 (Feb. 2009), pp. 195–205. DOI: 10.1016/j.actaastro.2008.07.019.

[26] Terry Fong. "Volatiles Investigating Polar Exploration Rover". In: *NASA Ames Research Center*. Mar. 2021. URL: https://ntrs.nasa.gov/api/citations/20210012662/downloads/viper-2021-03-29.pdf.

[27] J. Balaram, MiMi Aung, and Matthew P. Golombek. "The Ingenuity Helicopter on the Perseverance Rover". In: *Space Science Reviews* 217.4 (May 2021), p. 56. ISSN: 1572-9672. DOI: 10.1007/s11214-021-00815-w. URL: https://doi.org/10.1007/s11214-021-00815-w.

[28] Nadine Buhl, Martin Altenburg, and Markus Manns. "Sentinel-2A/B Thermal Design - Lessons Learnt from TBTV, LEOP and IOC". In: *International Conference on Environmental Systems* (2018). URL: http://hdl.handle.net/2346/74129.

[29] Philippe Martimort et al. "Sentinel-2 optical high resolution mission for GMES operational services". In: *2007 IEEE International Geoscience and Remote Sensing Symposium*. 2007, pp. 2677–2680. DOI: 10.1109/IGARSS.2007.4423394.

[30] Che-Shing Kang. "Multilayer Insulation for Spacecraft Applications". In: *Microsatellites as Research Tools*. Ed. by Fei-Bin Hsiao. Vol. 10. COSPAR Colloquia Series. Pergamon, 1999, pp. 175–179. DOI: https://doi.org/10.1016/S0964-2749(99)80023-7. URL: https://www.sciencedirect.com/science/article/pii/S0964274999800237.

[31] Marcel Veismann et al. "Low-density multi-fan wind tunnel design and testing for the Ingenuity Mars Helicopter". In: *Experiments in Fluids* 62.9 (Sept. 2021), p. 193. ISSN: 1432-1114. DOI: 10.1007/s00348-021-03278-5. URL: https://doi.org/10.1007/s00348-021-03278-5.

[32] Shannah Withrow-Maser et al. "An Advanced Mars Helicopter Design". In: *AIAA ASCEND*. 2020.

[33] Aerojet Rocketdyne. *In-Space Propulsion Data Sheets version 4.8.20*. https://satcatalog.s3.amazonaws.com/components/845/SatCatalog_-_Aerojet_Rocketdyne_-_MR-106L_22N_-_Datasheet.pdf?lastmod=20210710010020. 2022.

[34] Eckart Schmidt, Gerald Brewster, and George Cain. "Mars Lander Retro Propulsion". In: Oct. 1999.

[35] ArianeGroup GmbH Orbital Propulsion Center. *Hydrazine Propellant Tanks Overview*. https://www.space-propulsion.com/spacecraft-propulsion/hydrazine-tanks/hydrazine-tank-overview.html. 2020.

[36] G.P. Sutton and O. Biblarz. *Rocket Propulsion Elements*. John Wiley & Sons, 2010. ISBN: 9780470080245. URL: https://books.google.ch/books?id=1Sf6eV6CgtEC.

[37] Inc. Moog. *Rolling Diaphragm Tanks*. https://www.moog.com/content/dam/moog/literature/Space_Defense/spaceliterature/propulsion/moog-rolling-diaphragm-tanks-datasheet.pdf. 2013.

[38] Infinite Composites Technologies. *ICT Tank Specifications*. https://app.hubspot.com/documents/7946954/view/83846080?accessId=023a54. 2022.

[39] *Liquid Rocket Lines, Bellows, Flexible Hoses, and Filters. NASA SP-8123*. Vol. 8123. 1977.

[40] Muriel Richard. *Lecture notes in Spacecraft Design and System Engineering, Space Propulsion Subsystem*. Space Center EPFL, 2019.

[41] Ronald A. Spores, Robert Masse, and Scott Kimbrel. "GPIM AF-M315E Propulsion System". In: *50th AIAA/ASME/SAE/ASEE Joint Propulsion Conference Exhibit* (July 2013).

[42] Farzin Amzajerdian et al. "Imaging Flash Lidar for Autonomous Safe Landing and Spacecraft Proximity Operation". In: *NASA Langley Research Center, Hampton, Virginia, 23681* ().

[43] Georgios D. Tzeremes et al. "Altimetry, Imaging and Landing Location Selection Lidars for ESA Space Applications". In: *IGARSS 2019 - 2019 IEEE International Geoscience and Remote Sensing Symposium*. 2019, pp. 4775–4778. DOI: 10.1109/IGARSS.2019.8900519.

[44] Alexandre Pollini, Christophe Pache, and Jacques Haesler. "CSEM Space Lidars for Imaging and Rangefinding". In: *IGARSS 2018 - 2018 IEEE International Geoscience and Remote Sensing Symposium*. 2018, pp. 1849–1852. DOI: 10.1109/IGARSS.2018.8519241.

[45] Alexandre Pollini, Matteo Perenzoni, and Christophe Pache. *SPAD for space active debris removal and exploration*. https://www.imagesensors.org/Past20Workshops/202020ISSW/Alexandre_Pollini_ISSW2020_CSEM.pdf. International SPAD Sensor Workshop 2020, 2020.

[46] Muriel Richard. *Lecture notes in Spacecraft Design and System Engineering, Electrical Power System*. Space Center EPFL, 2019.

[47] ISISpace. *iEPS Type A, Type B and Type C Datasheet, ISIS-iEPS2$_0$ – DS – 00001, version1.0*. https://www.isispace.nl/wp-content/uploads/2019/04/ISIS-iEPS2_0-DS-00001-iEPS_Datasheet-1_0.pdf. 2019.

[48] Nacer Chahat et al. "Advanced CubeSat Antennas for Deep Space and Earth Science Missions: A review". In: *IEEE Antennas and Propagation Magazine* 61.5 (2019), pp. 37–46. DOI: 10.1109/MAP.2019.2932608.

[49] Alessandra Babuscia. "Telecommunication Systems for Small Satellites Operating at High Frequencies: A Review". In: *Information* 11.5 (2020). ISSN: 2078-2489. DOI: 10.3390/info11050258. URL: https://www.mdpi.com/2078-2489/11/5/258.

[50] J. (Bob) Balaram et al. "Mars Helicopter Technology Demonstrator". In: *2018 AIAA Atmospheric Flight Mechanics Conference* (Jan. 2018). DOI: 10.2514/6.2018-0023.

[51] Matthew W. Gerberich and Steven R. Oleson. "Estimation Model of Spacecraft Parameters and Cost Based on a Statistical Analysis of COMPASS Designs". In: *American Institute of Aeronautics and Astronautics* (2014).

[52] Jacob Job Wijker. *Spacecraft Structures*. Springer Berlin, Heidelberg, 2008. ISBN: 978-3-540-75552-4.

[53] Mark Shirley and Edward Balaban. *An Overview of Mission Planning for the VIPER Rover, NASA*. https://ntrs.nasa.gov/api/citations/20220008301/downloads/2022-06-02-spaceops-viper-planning.pdf. 2022.

[54] Matt Dawson et al. "Monopropellant Hydrazine 700 lbf Throttling Terminal Descent Engine for Mars Science Laboratory". In: *43rd AIAA/ASME/SAE/ASEE Joint Propulsion Conference & Exhibit*. DOI: 10.2514/6.2007-5481. eprint: https://arc.aiaa.org/doi/pdf/10.2514/6.2007-5481. URL: https://arc.aiaa.org/doi/abs/10.2514/6.2007-5481.

[55] Farzin Amzajerdian et al. "Lidar systems for precision navigation and safe landing on planetary bodies". In: *NASA Langley Research Center, Hampton, Virginia and Coherent Applications, Inc., Hampton, Virginia* (2011).

[56] Automation NASA Robotics and Control. *Gimbal for Steering Propelled CubeSats*. https://ntts-prod.s3.amazonaws.com/t2p/prod/t2media/tops/pdf/MFS-TOPS-74.pdf.

[57] Mark Sawley. *Lecture notes on Numerical Flow Simulation*. Ecole Polytechnique Fédérale de Lausanne (EPFL), 2019.

[58] Inc. ANSYS. *ANSYS Fluent Theory Guide, Release 15.0*. 2013.

[59] Inc. ANSYS. *ANSYS Fluent User's Guide, Release 17.2*. 2016.

[60] Garrett Shea and Brian Dunbar. *Systems Engineering Handbook, 5.3 Product Verification*. National Aeronautics and Space Administration, 2019.

[61] Marc Toussaint. *Lecture notes on Lessons Learned from Space Exploration*. Ecole Polytechnique Fédérale de Lausanne (EPFL), 2020.

[62] Qing Lin et al. "Investigation on soft landing impact test of scale lunar lander model". In: *Journal of Vibroengineering, Vol. 16, Issue 3* (May 2014), pp. 1114–1139.

[63] John Botsis. *Lecture notes on Structural Mechanics*. Ecole Polytechnique Fédérale de Lausanne (EPFL), 2018.

A Requirements

The full sets of the system's requirements, for the drone and the service station respectively, are shown in figures 43 and 44. The legend used for the subsystems is the following:

- COM: Communication
- CTRL: Flight control
- EPS: Electrical power system
- FUEL: Fuel and propellant storage
- IF: Interface
- MES: Measurements
- OBC: On board computer
- PROP: Propulsion
- STR: Structure
- SYS: Entire system
- TH: Thermal

The verification methods used for these requirements are [60]:

- Analysis: The use of mathematical modeling and analytical techniques to predict the suitability of a design to stakeholder expectations based on calculated data or data derived from lower system structure end product verifications.
- Demonstration: Showing that the use of an end product achieves the individual specified requirement.
- Inspection: The visual examination of a realized end product.
- Testing: The use of an end product to obtain detailed data needed to verify performance or provide sufficient information to verify performance through further analysis.

ID code	System	Short	Detailed description	Verification
REQ-DRN-COM-01	COM	Rover communication	The drone should always be in sight with the rover	Analysis
REQ-DRN-COM-02	COM	Com range	The communication range of the drone shall be at least 2 times the flight range	Testing
REQ-DRN-COM-03	COM	Hovering strategy	The flight shall ensure direct communication with the rover and household and flight data transmitted to the rover	Demonstration
REQ-DRN-CTRL-01	CTRL	Autonomous landing	The drone shall be capable of autonomous landing on the drone base	Testing
REQ-DRN-CTRL-02	CTRL	Autonomous flying	The drone shall be capable of autonomously following a predefined trajectory	Testing
REQ-DRN-CTRL-03	CTRL	Return to base	The drone shall be capable to abort its flight mission and return to the base autonomously	Testing
REQ-DRN-EPS-01	EPS	Power capacity	The power system shall provide all energy required for one flight (with contingency)	Testing
REQ-DRN-EPS-02	EPS	Rechargeability	The power system shall be rechargeable by the drone base	Testing
REQ-DRN-FUEL-01	FUEL	Propellant toxicity	The propulsion system should avoid the use of highly toxic propellants	Inspection
REQ-DRN-FUEL-02	FUEL	Refualability	The propulsion system shall be refualable by the drone base	Testing
REQ-DRN-FUEL-03	FUEL	Propellant freezing pt.	The propellant's freezing point shall be below -50°C	Testing
REQ-DRN-FUEL-04	FUEL	Pressurant freezing pt.	The pressurant's freezing point shall be below -50°C	Testing
REQ-DRN-FUEL-05	FUEL	Power during refueling	The power connection between the drone and the base shall be inactive during refueling	Demonstration
REQ-DRN-MES-01	MES	Obstacle detection	The drone should use the acquired 3D mapping data for obstacle detection and avoidance during flight	Testing
REQ-DRN-MES-02	MES	Altitude acquisition	The drone shall measure its altitude independently of the mapping sensor for object avoidance during flight	Testing
REQ-DRN-MES-03	MES	Position tracking	The drone shall track its position in space during flight	Testing
REQ-DRN-MES-04	MES	Payload mapping resolution	The payload shall provide a mapping resolution of <0.5 m/pixel	Demonstration
REQ-DRN-MES-05	MES	Mapping range	The drone's flight altitude shall be within the mapping range	Testing
REQ-DRN-MES-06	MES	Mapping technology	The mapping should be three-dimensional	Demonstration
REQ-DRN-MES-07	MES	Continuous mapping	The payload shall provide a continuous mapping under the flight path	Demonstration
REQ-DRN-MES-08	MES	Adaptability	The drone's payload should be interchangeable with instrumentation of similar size and power requirements	Testing
REQ-DRN-MES-09	MES	Landing location	The drone shall locate the landing pad when intitiating the landing maneuver	Testing
REQ-DRN-MES-010	MES	Dust on optics	The drone's optical instruments shall prevent dust to alter their precisions	Testing
REQ-DRN-OBC-01	OBC	Data storage inflight	3D mapping data shall be stored on the drone during the flight	Demonstration
REQ-DRN-OBC-02	OBC	Data transmission	3D mapping data shall be transmitted to the rover after landing on the base	Demonstration
REQ-DRN-OBC-03	OBC	Software update	The drone shall be able to return to the last known location in case of a loss of contact	Testing
REQ-DRN-PROP-01	PROP	Drone horizontal velocity	The maximum horizontal flight velocity shall lie below 50 m/s	Testing
REQ-DRN-PROP-02	PROP	Flight altitude	The drone shall flight at 50 m (± 10 m) during the mapping	Testing
REQ-DRN-PROP-03	PROP	Dust dispersion	The propulsion system shall not limit the mapping due to dust dispersion	Testing
REQ-DRN-PROP-04	PROP	Flight range	The propulsion system shall be capable of covering a horizontal distance of at least 1000 m	Testing
REQ-DRN-PROP-05	PROP	Thruster deformation	The thruster's nozzle shall be able to provide thrust during the entire flight without thermal plastic deformation	Testing
REQ-DRN-STR-01	STR	Storage size	The drone's volume shall fit within the drone base	Inspection
REQ-DRN-STR-02	STR	Mass & volume	The drone shall not exceed a mass of 20 kg	Demonstration
REQ-DRN-STR-03	STR	Structure deformation	The drone's structure shall not deform plastically	Testing
REQ-DRN-SYS-01	SYS	PL independence	The drone shall be independent of its payload	Demonstration
REQ-DRN-SYS-02	SYS	Dust proofness	The drone shall be completely dust proof against lunar regolith (equivalent rating: IP6)	Testing
REQ-DRN-SYS-03	SYS	Landing slopes	The drone shall be able to land on its base with inclinations up to 25°	Testing
REQ-DRN-SYS-04	SYS	Rover integration	The drone should deploy without help of an active onboard deployment mechanism on the rover	Demonstration
REQ-DRN-TH-01	TH	Stand-by temp.	The drone's thermal system shall keep the drone's temperature between [-20°C, 60°C] during stand-by phase with help of a radiation cover on the drone base	Testing
REQ-DRN-TH-02	TH	Thermal control	The drone shall be equipped with active thermal control	Demonstration
REQ-DRN-TH-03	TH	Operational temp.	The drone's and thermal system shall keep the drone's temperature between [0°C, 50°C] during operation phase	Testing
REQ-DRN-TH-04	TH	Sunlight time	The drone shall not stay in the sunlight for more than [TBD]	Analysis
REQ-DRN-TH-05	TH	Thermal control	The drone shall not stay in the swadow for more than [TBD]	Analysis

Figure 43: Drone's requirements

ID code	System	Short	Detailed description	Verification
REQ-BAS-COM-01	COM	Data reception & transmission	The base shall receive the drone's data and transmit it to the rover by cable	Testing
REQ-BAS-COM-02	COM	Com	The base shall send commands and receive flight and household data from the drone during the flight	Testing
REQ-BAS-IF-01	IF	Power interface	The base shall allow for the drone to be charged by the rover's power subsystem	Testing
REQ-BAS-IF-02	IF	Connection system	The base shall be equipped with a mechanically actuated connector system for the drone for power, propulsion and data	Testing
REQ-BAS-IF-03	IF	Standard interfaces	The base should be adapted to standard power, thermal and data interfaces to be defined by space agencies in the future	Demonstration
REQ-BAS-PROP-01	PROP	Propellant capacity	The base shall hold propellant tanks to refuel the drone's propellant tank at least 10 times	Demonstration
REQ-BAS-PROP-02	PROP	Pressurant capacity	The base shall hold pressurant tanks to refuel the drone's pressurant tank at least 10 times	Demonstration
REQ-BAS-STR-01	STR	Deflector	The base shall protect the rover from the drone's propulsion system	Testing
REQ-BAS-STR-02	STR	Hold-down mechanism	The base shall hold down the drone while in standby mode	Testing
REQ-BAS-TH-01	TH	Thermal protection	The base shall protect the drone from radiation and low temperatures	Testing

Figure 44: Service station's requirements

B Concept of operations

The full diagram of the concept of operations for the drone is shown in figure 45

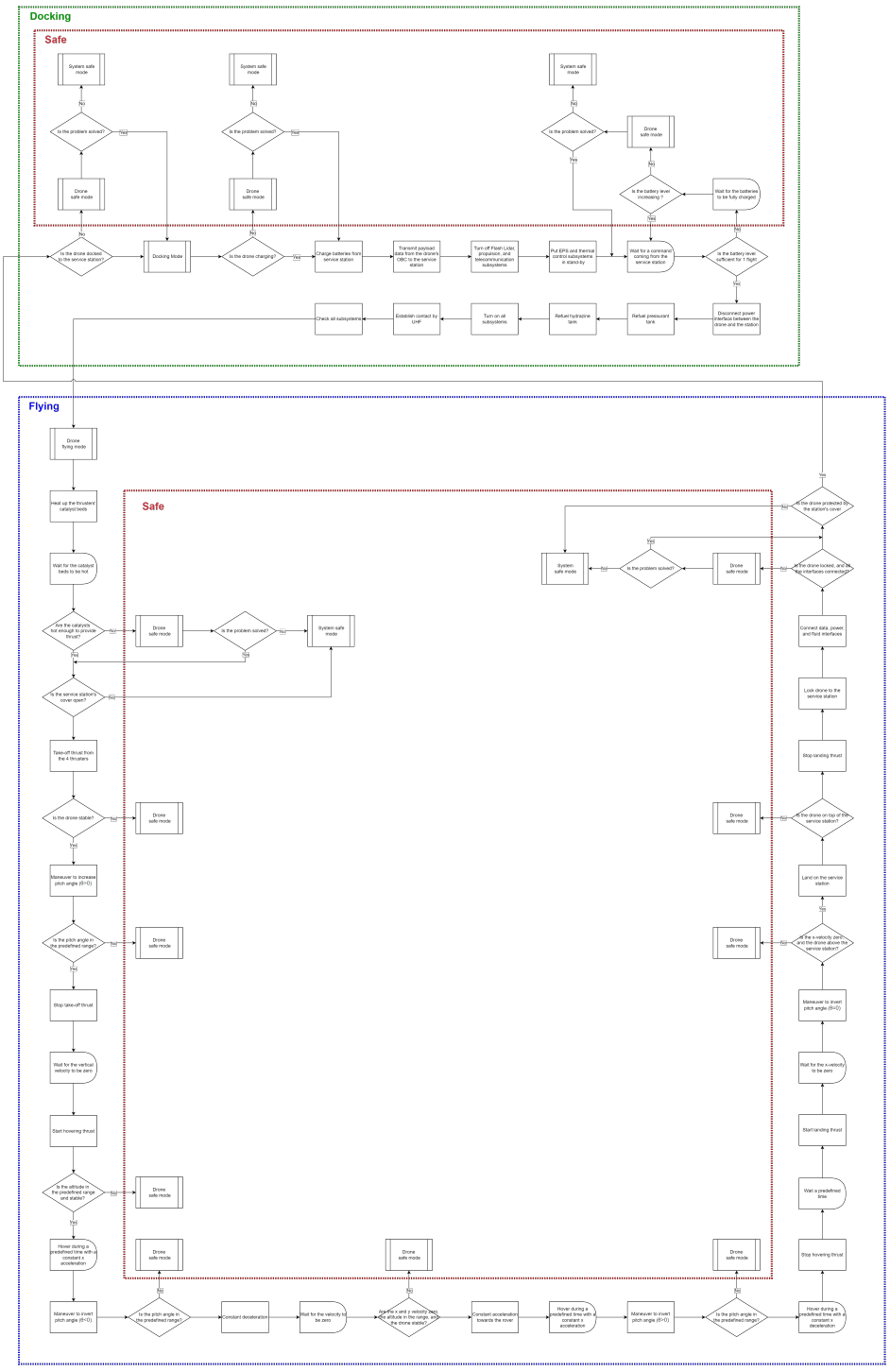

Figure 45: Drone's high level concept of operations

C Trade-off method

The goal of this section is to describe the method that was used for the different trade-offs throughout this thesis and illustrate it with an example.

The example shown here is a trade-off about the flight strategy, introduced in subsection 9.1. The first option is to fly with a zero pitch angle, but with four additional small thrusters dedicated to the horizontal trajectory control. The second option is to use four main thrusters, located in the top corners of the drone, which control both vertical but also horizontal movement by varying the pitch angle, as well as controlling the drone's attitude.

The method used in this analysis is derived from Marc Toussaint's trade-off method [61]. The first step is to define evaluation criteria for the specific example. For this analysis, they are listed below.

- Mass
- Complexity
- Fuel consumption
- Power consumption
- Failure risk
- Accuracy
- Testing required
- Simulation complexity
- Flight trajectory flexibility
- Cost
- Volume

All these evaluation criteria are then ranked by confronting each other, as shown in figure 46.

From the confrontation between the different predefined criteria, their adjusted importance can be derived as shown in figure 47.

Finally, a grade is attributed for every criterion and every potential solution. The grade is defined as

- 0: Poor performances
- 5: Average performances
- 10: Excellent performances

		Y Evaluation Criteria										
	Bottom left part: 3 = Y is much more important than X 2 = Y is more important than X 1 = Y is slightly more important than X 0 = Y is as important as X -1 = Y is slightly less important than X -2 = Y is less important than X -3 = Y is much less important than X	Mass	Complexity	Fuel consumption	Power consumption	Failure risk	Accuracy	Testing required	Simulation complexity	Flight trajectory flexibility	Cost	Volume
X Evaluation Criteria	Mass		-2	1	-2	-1	-1	-2	-3	-2	-2	-2
	Complexity	2		2	-1	1	0	-1	-2	0	1	-1
	Fuel consumption	-1	-2		-2	-1	-1	-2	-3	-2	-3	-2
	Power consumption	2	1	2		2	2	0	-1	1	2	1
	Failure risk	1	-1	1	-2		-1	-2	-3	-1	-1	-2
	Accuracy	1	0	1	-2	1		-1	-2	-1	0	-1
	Testing required	2	1	2	0	2	1		-1	1	2	1
	Simulation complexity	3	2	3	1	3	2	1		2	3	2
	Flight trajectory flexibility	2	0	2	-1	1	1	-1	-2		1	0
	Cost	2	-1	3	-2	1	0	-2	-3	-1		-1
	Volume	2	1	2	-1	2	1	-1	-2	0	1	

Figure 46: Confrontation between the different evaluation criteria

N =	11											SUM
	Sum	16	-1	19	-12	11	4	-11	-22	-3	4	-5	0
	Sum + (N-1)*3	46	29	49	18	41	34	19	8	27	34	25	330
	Adjusted Importance	0,1394	0,0879	0,1485	0,0545	0,1242	0,1030	0,0576	0,0242	0,0818	0,1030	0,0758	1
	Adjusted Importance (%)	13,94	8,79	14,85	5,45	12,42	10,30	5,76	2,42	8,18	10,30	7,58	100
	Rank	**2**	**6**	**1**	**10**	**3**	**4**	**9**	**11**	**7**	**4**	**8**	

Figure 47: Adjusted importance of the evaluation criteria

Figure 48, shows these grades, which are then multiplied by the adjusted importance defined earlier. A final score is attributed to each solution, which can then be ranked from the best suited to the defined problem to the least one.

		Pitch angle = 0; additional thrusters		Constant pitch angle ≠ 0; thruster angle ≠ 0	
Criteria	Adjusted importance	Grade	Adjusted grade	Grade	Adjusted grade
Mass	13,94	0	0	5	69,6969697
Complexity	8,79	0	0	5	43,93939394
Fuel consumption	14,85	10	148,4848485	5	74,24242424
Power consumption	5,45	5	27,27272727	10	54,54545455
Failure risk	12,42	0	0	5	62,12121212
Accuracy	10,30	10	103,030303	10	103,030303
Testing required	5,76	0	0	5	28,78787879
Simulation complexity	2,42	5	12,12121212	0	0
Flight trajectory flexibility	8,18	10	81,81818182	5	40,90909091
Cost	10,30	5	51,51515152	10	103,030303
Volume	7,58	0	0	5	37,87878788
Solution Score			424,2424242		618,1818182
Solution Ranking			**2**		**1**

Figure 48: Final grades of the different potential solutions for the trade-off

Note that this method provides a ranking between the solutions, nevertheless, a critical analysis shall be made from the result of this trade-off. For this example, the analysis and final result are shown in section 9.1.

D Risk Analysis

This section shows the full version of the failure mode and effects analysis that was introduced in section 6.

System	Subsystem	Failure mode	Failure mode reference number	Severity	Potential causes	Probability	Risk level	Mitigation	Flowback to requirements
Entire system	Entire system	The system is not ready on time	FAIL_SYS_1	3	Lidar not available	4	5	Also plan the mission and the Conops with different measurement instruments (for ex. investigate Lidar or optical camera with lightning)	REQ-DRN-SYS-01
				3	Late change in the design	5	6	Margin in the planning	
		Development cost is too high	FAIL_SYS_2	4	Unplanned costs due to new technologies	3	7	In the early phases take large margins for the cost budget (especially for payload)	
		Production cost is too high	FAIL_SYS_3	3	Too expensive material	3	4		
		Usage cost is too high	FAIL_SYS_4	2	To costly to take or extract fuel for multiple flights	2	2		
		The system is too heavy	FAIL_SYS_5	3	Lidar not lightweight enough	4	5	In the early phases take large margins for the mass budget (especially for payload)	
				3	The drone needs too much fuel to fly	4	5		
		One thruster loses the ability to provide thrust	FAIL_DRN_PROP_1	4	Fuel reservoir pressure too low	2	5	FAIL_DRN_FUEL_1	
				4	Pressurant reservoir pressure too low	2	5	FAIL_DRN_FUEL_4	
				4	Valve stuck closed	2	5	Add redundant valves	
				4	Mechanism overheating	4	8	In-depth thermal simulations	REQ-DRN-TH-01; REQ-DRN-TH-03; REQ-DRN-TH-04; REQ-DRN-TH-05
				4	Mechanism underheated	3	7	In-depth thermal simulations	REQ-DRN-TH-01; REQ-DRN-TH-03; REQ-DRN-TH-04; REQ-DRN-TH-05
				4	Power supply problem	2	5	Add redundant power cables	
				4	Software problem	2	5	FAIL_DRN_OBC_4	
		Two or more thrusters lose the ability to provide thrust	FAIL_DRN_PROP_2	5	Fuel reservoir pressure too low	2	8	FAIL_DRN_FUEL_1	
				5	Pressurant reservoir pressure too low	2	8	FAIL_DRN_FUEL_4	
				5	Multiple valve stuck closed	1	5		
				5	Mechanism overheating	4	11	In-depth thermal simulations	REQ-DRN-TH-01; REQ-DRN-TH-03; REQ-DRN-TH-04; REQ-DRN-TH-05

Figure 49: FMEA 1/8

	Propulsion			5	Mechanism underheated	3	10	In-depth thermal simulations	REQ-DRN-TH-01; REQ-DRN-TH-03; REQ-DRN-TH-04; REQ-DRN-TH-05
				5	Multiple power supply problem	1	5		
				5	Software problem	1	5	FAIL_DRN_OBC_4	
		One thruster provides thrust in an uncontrollable way	FAIL_DRN_PROP_3	4	Fuel reservoir pressure too high	2	5	FAIL_DRN_FUEL_2	
				4	Pressurant reservoir pressure too high	2	5	FAIL_DRN_FUEL_5	
				4	Valve leakeage	3	7	Add multiple ways to isolate the valves and use the redundant ones	
				4	Control algorithm problem	2	5	FAIL_DRN_CTRL_1; FAIL_DRN_CTRL_2; FAIL_DRN_CTRL_3; FAIL_DRN_CTRL_4; FAIL_DRN_CTRL_5	
				4	Software problem	2	5	FAIL_DRN_OBC_4	
		Two or more thrusters provide thrust in an uncontrollable way	FAIL_DRN_PROP_4	5	Fuel reservoir pressure too high	2	8	FAIL_DRN_FUEL_2	
				5	Pressurant reservoir pressure too high	2	8	FAIL_DRN_FUEL_5	
				5	Multiple valve leakeage	2	8	Add multiple ways to isolate the valves and use the redundant ones	
				5	Control algorithm problem	1	5	FAIL_DRN_CTRL_1; FAIL_DRN_CTRL_2; FAIL_DRN_CTRL_3; FAIL_DRN_CTRL_4; FAIL_DRN_CTRL_5	
				5	Software problem	1	5	FAIL_DRN_OBC_4	
		One thruster does not exhaust gas in the axial direction	FAIL_DRN_PROP_5	3	Deformed nozzle due to overheating	3	4	Perform in depth thermal simulation and select appropriate material with margin	REQ-DRN-PROP-05
				3	Damaged nozzle due to meteorit impact	1	2		
		Two or more thrusters do not exhaust gas in the axial direction	FAIL_DRN_PROP_6	4	Deformed nozzle due to overheating	3	7	Perform in depth thermal simulation and select appropriate material with margin	REQ-DRN-PROP-05
				4	Damaged nozzle due to meteorit impact	1	3		
		Drone's fuel reservoir pressure is too low	FAIL_DRN_FUEL_1	3	Problem during refuelling	3	4	Intensive interface mechnism testing	
				3	Reservoir temperature too low	4	5	Perform in depth thermal simulation	REQ-DRN-TH-01; REQ-DRN-TH-03; REQ-DRN-TH-04; REQ-DRN-TH-05

Figure 50: FMEA 2/8

	Fuel storage	Drone's fuel reservoir pressure is too high	FAIL_DRN_FUEL_2	4	Problem during refueling	3	7	Intensive interface mechnism testing	
				4	Reservoir temperature too high	4	8	Perform in-depth thermal simulation	REQ-DRN-TH-01; REQ-DRN-TH-03; REQ-DRN-TH-04; REQ-DRN-TH-05
		Drone's fuel quantity is decreasing abnormally during flight	FAIL_DRN_FUEL_3	3	Leakage in the reservoir	2	3	Large safety margin for the reservoir's thickness and intensive testing	
				3	Leakage in the fuel lines	3	4	Add large safety margin for the fuel lines	
		Drone's pressurant pressure is too low	FAIL_DRN_FUEL_4	2	Problem during refueling	3	2	Intensive interface mechnism testing	
				2	Reservoir temperature too low	4	3	Perform in depth thermal simulation	REQ-DRN-TH-01; REQ-DRN-TH-03; REQ-DRN-TH-04; REQ-DRN-TH-05
		Drone's pressurant pressure is too high	FAIL_DRN_FUEL_5	3	Problem during refueling	3	4	Intensive interface mechnism testing	
				3	Reservoir temperature too high	4	5	Perform in depth thermal simulation	REQ-DRN-TH-01; REQ-DRN-TH-03; REQ-DRN-TH-04; REQ-DRN-TH-05
		Drone's pressurant quantity is decreasing abnormally during flight	FAIL_DRN_FUEL_6	3	Leakage in the reservoir	2	3	Large safety margin for the reservoir's thickness and intensive testing	
				3	Leakage in the fuel lines	3	4	Add large safety margin for the fuel lines	
		Fire during refuelling	FAIL_DRN_FUEL_7	4	Spark generated by the power system while refueling	3	7	Isolate battery charging and refueling	REQ-DRN-FUEL-05
		The drone is unable to return to the base	FAIL_DRN_CTRL_1	5	Thruster issue	3	10	FAIL_DRN_PROP_1; FAIL_DRN_PROP_2; FAIL_DRN_PROP_3; FAIL_DRN_PROP_4; FAIL_DRN_PROP_5; FAIL_DRN_PROP_6	
				5	Control algorithm not well designed	2	8	Intensive control algorithm testing; Constant health check and early switch to safe mode in case of any anomaly	
				5	Navigation sensors not accurate enough	1	5		
				5	Uncalibrated sensors	2	8	Full sensor calibration during the first flight and calibration check before every flight	
				5	Damaged electronics	2	8	FAIL_DRN_OBC_1; FAIL_DRN_OBC_2; FAIL_DRN_OBC_3; FAIL_DRN_OBC_4	
				5	Dust on the sensors	3	10	Intensive testing of the flame diverter; very low friction coating	
		The drone is unable	FAIL_DRN_CTRL_2	4	Thruster issue	3	7	FAIL_DRN_PROP_1; FAIL_DRN_PROP_2; FAIL_DRN_PROP_3; FAIL_DRN_PROP_4; FAIL_DRN_PROP_5; FAIL_DRN_PROP_6	
				4	Control algorithm not well designed	2	5	Intensive control algorithm testing; Constant health check and early switch to safe mode in case of any anomaly	

Figure 51: FMEA 3/8

Drone	Flight Control	to maintain attitude	FAIL_DRN_CTRL_2	4	Damaged electronics	2	5	FAIL_DRN_OBC_1; FAIL_DRN_OBC_2; FAIL_DRN_OBC_3; FAIL_DRN_OBC_4		
				4	Dust on the sensors	3	7	Intensive testing of the flame diverter; very low friction coating		
		The drone is unable to follow the predefined trajectory	FAIL_DRN_CTRL_3	3	Thruster issue	3	4	FAIL_DRN_PROP_1; FAIL_DRN_PROP_2; FAIL_DRN_PROP_3; FAIL_DRN_PROP_4; FAIL_DRN_PROP_5; FAIL_DRN_PROP_6		
				3	Control algorithm not well designed	2	3	Intensive control algorithm testing; Constant health check and early switch to safe mode in case of any anomaly		
				3	Damaged electronics	2	3	FAIL_DRN_OBC_1; FAIL_DRN_OBC_2; FAIL_DRN_OBC_3; FAIL_DRN_OBC_4		
				3	Dust on the sensors	3	4	Intensive testing of the flame diverter; very low friction coating		
		The drone hits an obstacle	FAIL_DRN_CTRL_4	4	Invisible obstacle on the planned trajectory	2	5	Need to plan every flight with large distance margin from the obstacles		
		The drone is unable to land on the base	FAIL_DRN_CTRL_5	5	Dust on the tracking lights	4	11	Put the lights higher than the base so that they emerge in case of dust; intensive testing of the flame diverter; very low friction coating	REQ-DRN-MES-010	
				5	Dust on the optical camera	3	10	Investigate gas spray on the camera optics; intensive testing of the flame diverter; very low friction coating	REQ-DRN-MES-09	
				5	Thruster issue	2	8	FAIL_DRN_PROP_1; FAIL_DRN_PROP_2; FAIL_DRN_PROP_3; FAIL_DRN_PROP_4; FAIL_DRN_PROP_5; FAIL_DRN_PROP_6		
				5	Control algorithm not well designed	2	8	Intensive control algorithm testing; Constant health check and early switch to safe mode in case of any anomaly		
	Measurment	The Lidar provides unaccurate or false data	FAIL_DRN_MES_1	5	Dust on the Lidar	3	10	Investigate gas spray on the Lidar optics; intensive testing of the flame diverter; very low friction coating		
				5	Software problem	2	8	Intensive software testing; possibility to uplink software updates if needed		
				5	Uncalibrated Lidar	1	5	Full sensor calibration during the first flight and calibration check before every flight		
		The mapping resolution is not high enough	FAIL_DRN_MES_2	4	Dust on the Lidar	3	7	Investigate gas spray on the Lidar optics; intensive testing of the flame diverter; very low friction coating		
				4	Unable to maintain altitude	2	5	FAIL_DRN_CTRL_2		
		Housekeeping data is false or missing	FAIL_DRN_OBC_1	3	Software problem	2	3	Implement a secondary flight software in case of a failure with the main one; possibility for software update	REQ-DRN-OBC-03	
				3	Loss of communication between subsystems	3	4			
		OBC fails on the	FAIL_DRN_OBC_2	3	Software problem	2	3	Implement a secondary flight software in case of a failure with the main one; possibility for software update		

Figure 52: FMEA 4/8

		base	FAIL_DRN_OBC_2	3	Damaged electronics	2	3		
	OBC	OBC fails in flight	FAIL_DRN_OBC_3	4	Software problem	2	5	Implement a secondary flight software in case of a failure with the main one; possibility for software update	
				4	Damaged electronics	2	5		
		Software failure	FAIL_DRN_OBC_4	4	Radiation induced problem	3	7	Radiation hardened components and radiation cover in the base	
				4	Software stuck in infinite loop	3	7	Possibility to force a switch to the safe mode from the ground station	
				4	Software unable to enter safe mode	2	5	Implement a secondary flight software in case of a failure with the main one; possibility for software update	
	EPS	Battery voltage is too low on the base	FAIL_DRN_EPS_1	2	Battery charge time was too low	3	2		
				2	Too many battery cycles	3	2		
		Battery voltage is too low in flight	FAIL_DRN_EPS_2	4	Initial battery voltage was too low	1	3		
				4	Battery drain	3	7	Add redundant batteries for contingency	
		One or more subsystems do not recieve enough power	FAIL_DRN_EPS_3	4	Battery voltage is too low	2	5		
				4	Damaged power distribution cables	2	5	Add redundant power cables	
		Battery voltage does not go up on the base	FAIL_DRN_EPS_4	4	Dust on the power connector	4	8	Put the connectors higher than the base so that they emerge in case of dust; intensive testing of the flame diverter; investigate movable hatch	
				4	Damaged connector	2	5		
	Communication	Drone is unable to communicate with the base during flight	FAIL_DRN_COM_1	3	Drone out of sight	3	4	Implement a function to return to the last known position in the flight control algorithm	REQ-DRN-OBC-03
				3	Damaged antenna	3	4		
		Drone is unable to communicate on the base	FAIL_DRN_COM_2	4	Damaged connector	2	5		
				4	Software problem	2	5		
				4	Flight time in sunlight is too long	2	5	In-depth thermal simulations and large margin for the maximum time in sunlight	REQ-DRN-TH-01; REQ-DRN-TH-03; REQ-DRN-TH-04; REQ-DRN-TH-05

Figure 53: FMEA 5/8

	Thermal	The temperature of one or more subsystems is too high during flight	FAIL_DRN_TH_1	4	Bad thermal design	3	7	In-depth thermal simulations and testing	REQ-DRN-TH-01; REQ-DRN-TH-03; REQ-DRN-TH-04; REQ-DRN-TH-05
				4	Too much heat generated internally from the subsystem	3	7	In-depth thermal simulations and testing; put the most critical parts near the radiators	REQ-DRN-TH-01; REQ-DRN-TH-03; REQ-DRN-TH-04; REQ-DRN-TH-05
		The temperature of one or more subsystems is too low during flight	FAIL_DRN_TH_2	4	Damaged heat straps	2	5		
				4	Bad thermal design	3	7	Put the critical components in a "warm electronic box"	
		The temperature of one or more subsystems is too high on the base	FAIL_DRN_TH_3	4	Base not sealed because of dust	4	8	Intensive testing of the flame diverter to avoid dust deposition; low friction coating	
				4	Bad base cover thermal design	3	7	In-depth thermal simulations and testing	REQ-DRN-TH-01; REQ-DRN-TH-03; REQ-DRN-TH-04; REQ-DRN-TH-05
				4	Too much heat generated internally from the subsystem	3	7	In-depth thermal simulations and testing; put the most critical parts near the radiators	REQ-DRN-TH-01; REQ-DRN-TH-03; REQ-DRN-TH-04; REQ-DRN-TH-05
		The temperature of one or more subsystems is too low on the base	FAIL_DRN_TH_4	3	Base not sealed because of dust	4	5	Intensive testing of the flame diverter to avoid dust deposition; low friction coating	
				3	Damaged base cover heater	3	4		
		Heat is not distibuted normally	FAIL_DRN_TH_5	3	Bad thermal design	3	4		
				3	Damaged heat straps	2	3		
		Heat is not evacuated normally	FAIL_DRN_TH_6	4	Bad thermal design	3	7	Add margin on the base radiator and add redundant heaters	
				4	Damaged radiator	1	3		
	Cover	The drone is not connected to the base	FAIL_BAS_COV_1	5	Unaccurate drone landing	3	10	FAIL_DRN_CTRL_5	
				5	Damaged locking mechanism	2	8	Intensive testing of the locking mechanisms; design holes in the landing pad to guide the drone for landing	
		The drone locking mechanism is stuck open	FAIL_BAS_COV_2	4	Dust impedes closing	4	8	Intensive testing of the flame diverter to avoid dust deposition; low friction coating	
				4	Damaged locking mechanism	2	5	Intensive testing of the locking mechanisms; design holes in the landing pad to guide the drone for landing	
		The drone locking mechanism is stuck closed	FAIL_BAS_COV_3	5	Power supply failure	2	8	Add redundant power cables	
				5	Damaged locking mechanism	2	8	Intensive testing of the locking mechanisms; design holes in the landing pad to guide the drone for landing	

Figure 54: FMEA 6/8

Base	Cover	Base cover is stuck open	FAIL_BAS_COV_4	4	Dust impedes closing	4	8	Intensive testing of the flame diverter to avoid dust deposition; low friction coating	
				4	Damaged mechanism	2	5	Intensive testing of the mechanism; margin in the required torque	
		Base cover is stuck closed	FAIL_BAS_COV_5	5	Power supply failure	2	8	Add redundant power cables	
				5	Damaged mechanism	2	8	Intensive testing of the mechanism; margin in the required torque	
		Base cover is not dustproof	FAIL_BAS_COV_6	3	Dust trapped during closing	4	5	Intensive testing of the flame diverter to avoid dust deposition; low friction coating	
				3	Meteorit impact	1	2		
	Thermal	The base temperture is too high	FAIL_BAS_TH_1	4	Bad heat dissipation design	3	7	In-depth thermal simulations and testing	
				4	Too much heat generated internally	2	5	In-depth thermal simulations and testing; put the most critical parts near the radiators	
		The base temperature is too low	FAIL_BAS_TH_2	3	Damaged heaters	2	3		
				3	Power supply problem	2	3		
	Fuel storage	Fuel reservoir pressure is too low	FAIL_BAS_FUEL_1	2	Problem during refueling	3	2	Intensive interface mechnism testing	
				2	Reservoir temperature too low	4	3	Perform in depth thermal simulation	
				2	Valve stuck open	3	2	Add multiple ways to isolate the valves and use the redundant ones	
		Fuel reservoir pressure is decreasing abnormally	FAIL_BAS_FUEL_2	4	Leakage in the reservoir	2	5	Large safety margin for the reservoir's thickness and intensive testing	
		Fuel reservoir pressure is too high	FAIL_BAS_FUEL_3	3	Problem during refueling	3	4	Intensive interface mechnism testing	
				3	Reservoir temperature too high	4	5	Perform in depth thermal simulation	
		Fuel is not distributed to the drone	FAIL_BAS_FUEL_4	4	Leakage in the fuel lines	2	5	Add large safety margin for the fuel lines	
				4	Valve stuck closed	2	5	Add redundant valves	
				2	Problem during refueling	3	2	Intensive interface mechnism testing	

Figure 55: FMEA 7/8

		Pressurant reservoir pressure is too low	FAIL_BAS_FUEL_5	2	Reservoir temperature too low	4	3	Perform in depth thermal simulation	
				2	Valve stuck open	2	2	Add multiple ways to isolate the valves and use the redundant ones	
		Pressurant reservoir pressure is decreasing abnormally	FAIL_BAS_FUEL_6	3	Leakage in the reservoir	2	3	Large safety margin for the reservoir's thickness and intensive testing	
		Pressurant reservoir pressure is too high	FAIL_BAS_FUEL_7	3	Problem during refueling	3	4	Intensive interface mechnism testing	
				3	Reservoir temperature too high	4	5	Perform in depth thermal simulation	
		Pressurant is not distributed to the drone	FAIL_BAS_FUEL_8	4	Leakage in the fuel lines	2	5	Add large safety margin for the fuel lines	
				4	Valve stuck closed	2	5	Add redundant valves	
	OBC	The base is unable to process the mapping data	FAIL_BAS_OBC_1	5	Corrupted, unprecise or wrong data	3	10	FAIL_DRN_MES_1	
				5	Software problem	2	8	Intensive software testing; possibility to uplink software updates if needed	
				5	Damaged connector	2	8	Intensive testing of the connector; design holes in the landing pad to guide the drone for landing	
		The base is unable to receive housekeeping data from the drone	FAIL_BAS_OBC_2	4	Drone out of sight	2	5	Implement a function to return to the last known position in the flight control algorithm	
				4	Damaged antenna	3	7	Place the antenna far from the flames to minimize the damage risk	
	EPS	Battery voltage is too low	FAIL_BAS_EPS_1	3	Power supply problem	2	3		
				3	Too much battery cycles	4	5	Add redundant batteries and large margin in the depth of discharge	
		The base is unable to provide power to the drone	FAIL_BAS_EPS_2	5	Damaged connector	2	8	Intensive testing of the connector; design holes in the landing pad to guide the drone for landing	
				5	Dust on the connector	3	10	Put the connector higher than the base so that they emerge in case of dust; intensive testing of the flame diverter; investigate movable hatch	
External	External	Lightweight Lidar's TRL is not high enough	FAIL_EXT_1	3	Too optimistic timeline	4	5	Margin in the timeline	
		Unrelated critical event (pandemic, war, economic crisis...)	FAIL_EXT_2	4	Unrelated critical event (pandemic, war, economic crisis...)	2	5		

Figure 56: FMEA 8/8

E Tank sizing calculations

Based on the volume and storage pressure of the fuel and pressurant, this section's goal is to obtain an estimate of the minimum thickness and mass of the corresponding tanks. From the flight simulation (section 9), $2.8kg$ of hydrazine is needed for one flight (taking 50% of margin), which corresponds to $2.75L$, which is stored at $2.4MPa$ [2].

To know how much pressurant is needed, the estimation given by Sutton et al. in Rocket Propulsion Elements [36] is used, as well as the analysis made during last semester [2]. The operating conditions are given by an ambient temperature of $298K$ and a storage pressure of the pressurant of $14MPa$. In this system, helium is used as the pressurant. With P_p and P_0 the storage pressures of propellant and pressurant, V_p the volume of propellant, and γ the heat capacity ratio, the pressurant volume needed (V_0) is then given by

$$V_0 = \frac{P_p}{P_p} \cdot V_p \cdot \left(\frac{\gamma}{1 - \frac{P_p}{P_0}} \right) = \frac{2.4}{14} \cdot 2.74 \cdot \left(\frac{\frac{5}{3}}{1 - \frac{2.4}{14}} \right) = 0.945L$$

The corresponding mass, using the ideal gas law, is $0.154kg$.

Knowing the volume taken by each fluid, the minimum tank radius is given by

$$R_{tank} = \sqrt[3]{\frac{3V}{4\pi}}$$

Which gives a radius of $R_{hydrazine} = 0.0868m$ and $R_{He} = 0.0609m$ for the fuel and pressurant tanks.

The material that is usually used for tanks with similar application is titanium [36], with the following properties for the maximum allowable stress ($\sigma = 900 \cdot 10^6\, N \cdot m^{-2}$), and the density ($\rho = 4.43 \cdot 10^3\, kg \cdot m^{-3}$).

The minimum thickness t, with a safety factor of S=5, is then given by

$$t = \frac{P \cdot R}{2 \cdot \sigma} \cdot S$$

which gives a thickness of $0.58\,mm$ for the hydrazine tank and $2.4\,mm$ for the pressurant one. Their corresponding mass is then given by $m = \rho \cdot \frac{4}{3}\pi \cdot (R^3 - (R-t)^3)$. Using this approach, the minimum mass for the fuel tank is $0.2412\,kg$, and $0.4762\,kg$ for the pressurant one.

F Structural calculations

In section 8.2.7, a requirement for the structure was defined based on Ingenuity's one [50]. It states that the structure shall not deform plastically in the event of a drop from $0.5m$ above the Moon's surface. This section introduces a simple structural model to determine the sizing of the carbon fiber plates used in the satellite.

As mentioned in section 8.2.7, the structure is composed of three main parts, two horizontal plates, one on top and one on the bottom side, and a vertical one linking the structure together. The simplification of this structure is presented in the left part of figure 57. In this analysis, the assumption is made that during the fall, as all the components are attached to these structural parts, the force is then applied in the center of the lower plate, through the vertical one.

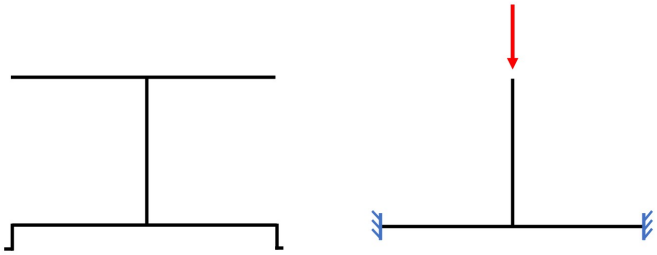

Figure 57: Simplified model of the structure (side view)

The structure can then be split into two main parts, as shown in figure 58. On the left, the lower plate is analyzed in bending, as the vertical plate is buckling.

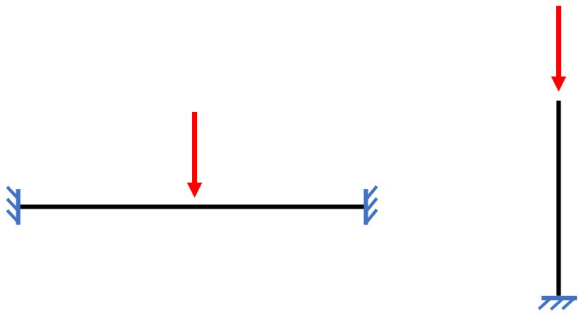

Figure 58: Decomposition of the structure for the bending analysis (left) and the bucking (right)

From the conservation of mechanical energy, if the drone drops from an altitude of $0.5m$, the impact velocity is given by

$$v_{impact} = \sqrt{2 \cdot g \cdot \Delta h} = 1.273\, m \cdot s^{-1}$$

In lunar landing tests [62], it was found that the time of impact, during which the drone will be in contact with the floor, is in the order of magnitude of 0.1s, this value is kept for this preliminary calculations.

The average force, coming from the average deceleration, is then given by

$$F_{avg} = m \cdot \frac{\Delta v}{\Delta t} = 190.9\, N$$

This average impact force will then be used in the following structural analysis.

F.1 Bending

This subsection presents the bending analysis of the lower plate [63]. In the preliminary design, this plate is in carbon fiber, with the following dimensions and properties

- length: L = 360mm
- width: w = 40mm
- height: h = 1mm
- Yield strength: Y = 2500MPa
- Young's modulus: E = 500GPa

The moment of inertia is the $I = \frac{w \cdot h^3}{12} = 3.33 \cdot 10^{-12}\, kg \cdot m^{-2}$. If x represents the horizontal variable, starting from the left of the structure (figure 58), the beam deflection on the left half is then

$$\delta = \frac{F \cdot x^2}{48 \cdot E \cdot I} \cdot (3L - 4x)$$

The maximum deflection in the center of the plate is

$$\delta = \frac{F \cdot L^3}{192 \cdot E \cdot I} = 2.79 \cdot 10^{-2}\, m$$

The bending stress is

$$\sigma_{bending} = \frac{F}{A} = 4.77\, MPa$$

This bending stress is much smaller than the yield strength of carbon fiber, therefore, the characteristics of this horizontal plate are suitable for a drop of $0.5m$ without suffering from plastic deformation.

F.2 Buckling

The second part of this structural analysis is shown in the right part of figure 58, with the potential bucking of the vertical beam.

The initial dimensions of this plate are the same as the horizontal one, the moment of inertia is therefore also the same.

The buckling load is given by

$$\sigma_{buckling} = \frac{F}{A} = 4.77\,MPa$$

The critical load for buckling is given by Euler's equation

$$\sigma_{cr} = \frac{F_{cr}}{A} = \frac{4\pi \cdot E \cdot I}{L^2 \cdot A} = 4.04\,MPa$$

In the case of a $0.5m$ drop, the actual load is higher than the critical load for buckling. Then, if the same material is kept, the area has to be increased. The same beam with a doubled thickness ($2mm$) is then taken. The moment of inertia becomes $I = \frac{w \cdot h^3}{12} = 2.67 \cdot 10^{-11}\,kg \cdot m^{-2}$. Using the previous equations, the buckling load is $\sigma_{buckling} = 2.39\,MPa$, and the critical buckling becomes $\sigma_{cr} = 16.18\,MPa$. The vertical plate will therefore not undergo buckling in this case, with a safety factor of 6.77.

G Flight simulation model

The full version of the model used for the flight simulation discussed in section 9 is shown in figure 59.

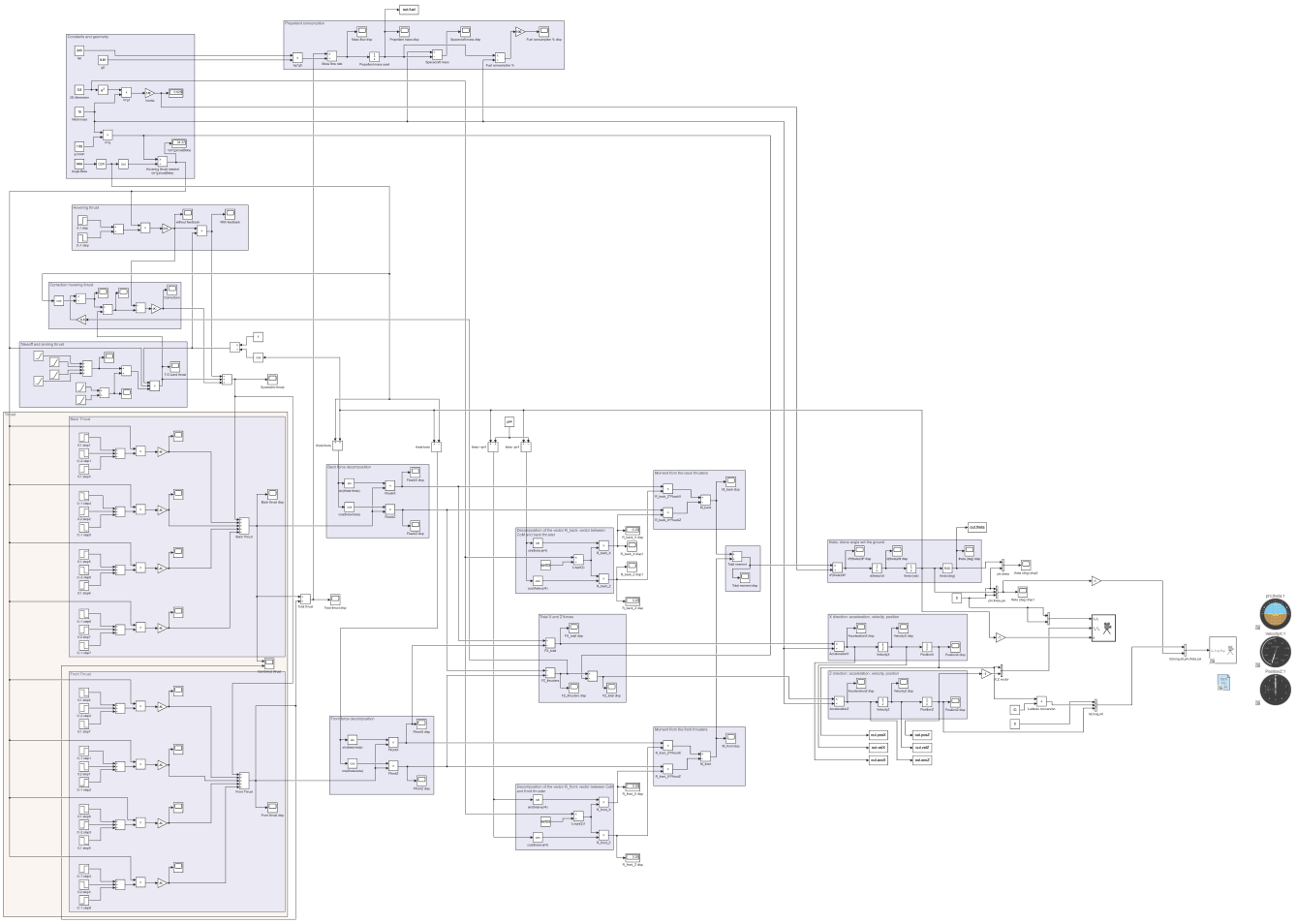

Figure 59: Simulink model used for the flight simulation

H Flight simulation example

The additional results obtained from the example in section 9.3 are shown in the following figures

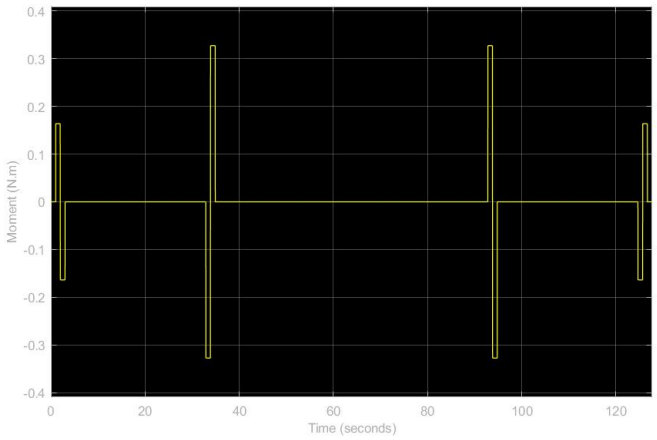

Figure 60: Total moment applied at the center of gravity of the drone

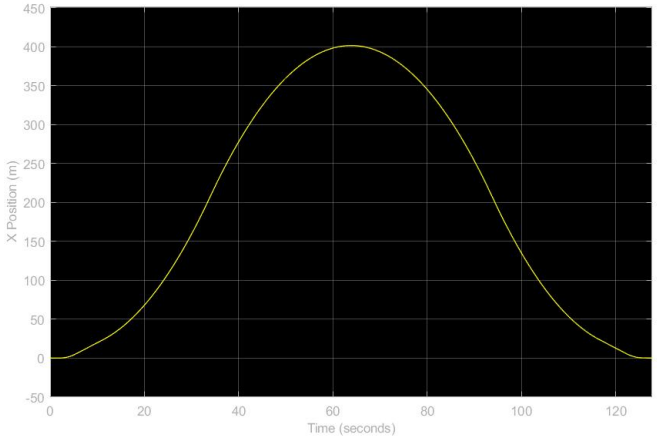

Figure 61: Horizontal position of the drone

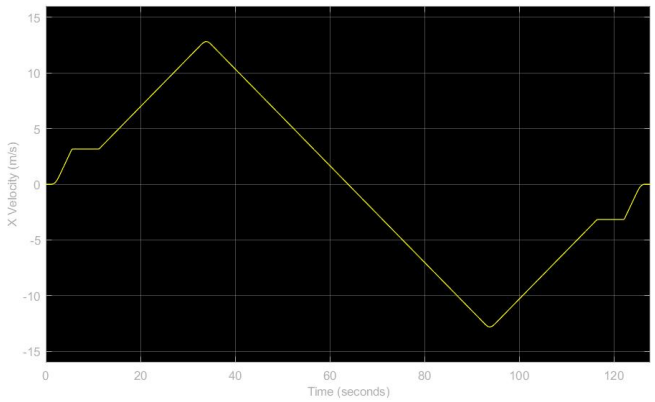

Figure 62: Horizontal velocity of the drone

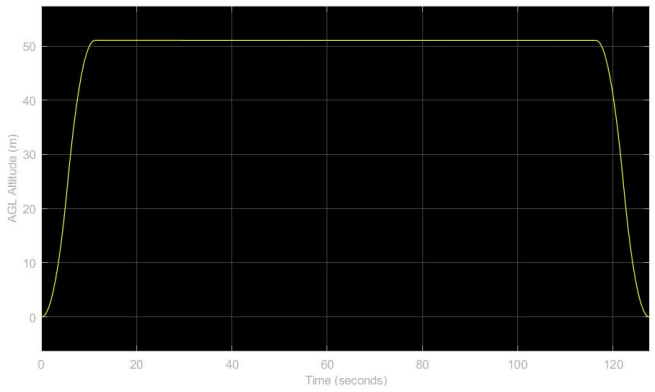

Figure 63: Vertical position of the drone

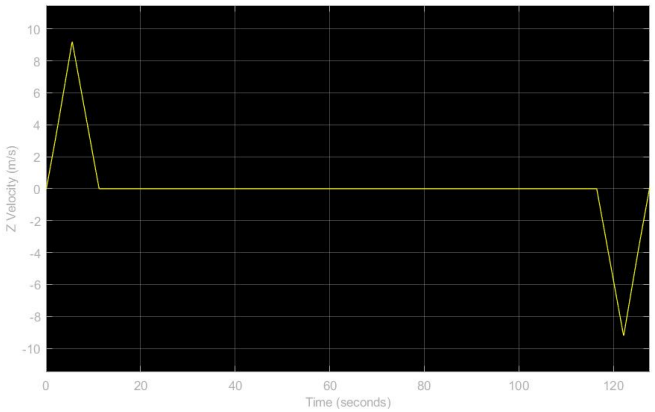

Figure 64: Vertical velocity of the drone